GENERATION AND CHARACTERIZATION OF THREE DIMENSIONAL ORGANOTYPIC KID SYNDROME SKIN MODEL

A Thesis Submitted to
the Graduate School of Engineering and Sciences of
İzmir Institute of Technology
in Partial Fulfillment of the Requirements for the Degree of

MASTER OF SCIENCE

in Molecular Biology and Genetic

by
Özgür ÖZTÜRK

July 2017
İZMİR

We approve the thesis of **Özgür ÖZTÜRK**

Examining Committee Members

_____
Assist. Prof. Dr. Gülistan MEŞE ÖZÇİVİCİ
Department of Molecular Biology and Genetics, Izmir Institute of Technology

_____
Assoc. Prof. Dr. Özden YALÇIN ÖZUYSAL
Department of Molecular Biology and Genetics, Izmir Institute of Technology

_____
Assist. Prof. Dr. Yavuz OKTAY
Izmir International Biomedicine and Genome Institute, Dokuz Eylül University

25 July 2017

_____
Assist. Prof. Dr. Gülistan MEŞE ÖZÇİVİCİ
Supervisor, Molecular Biology and Genetics,
Izmir Institute of Technology

_____
Prof. Dr. Volkan SEYRANTEPE
Head of Department of Molecular
and Genetics

_____
Prof. Dr. Aysun SOFUOĞLU
Dean of the Graduate School of
Biology Engineering and Sciences

ACKNOWLEDGEMENTS

I would like to thank my supervisor Assist. Prof. Gülistan Meşe Özçivici for her guidance, patience and help and contributions during my graduate work. I am also thankful to all my friends in Meşe-Özçivici Lab for their kindness and help. I also would like to thank Assoc. Prof. Dr. Engin ÖZÇİVİCİ and Assoc. Prof. Dr. Özden YALÇIN ÖZUYSAL for their support and contributions. Finally, I would like to give my sincere thanks to Şurhan GÖL for always being besides me and to my family for their support through my education.

ABSTRACT

GENERATION AND CHARACTERIZATION OF THREE DIMENSIONAL ORGANOTYPIC KID SYNDROME SKIN MODEL

Keratitis, ichthyosis, deafness (KID) syndrome is a rare genetic disorder caused by connexin 26 gene mutation that shows quite debilitating and horrific effects on patients. Syndrome itself is complex and 2D culture methods fail to provide complex and close to real conditions to investigate KID syndrome. Our goal is to construct organotypic 3D skin model for the KID syndrome. First of all, stable cell lines expressing wild type and D50Y mutant Cx26 protein were generated. Immunostaining, Western blot and qRT-PCR analysis confirmed Cx26 expression in stable cell lines, meaning these cell lines can be utilized to construct 3D skin model. In order to generate organotypic KID syndrome skin models, commercially available transwell inserts were used. Constructs were prepared by plating fibroblast-collagen mixture in inserts and then plating generated stable cell lines on top of the fibroblast-collagen layer. Then immunostaining was performed on generated skin constructs. Immunostaining of cytokeratin 14 confirmed that 3D model has basal layer of the epidermis. Also, KID skin model with Whatman paper was conducted as an alternative to transwell inserts. Phalloidin staining results showed that generated cell lines formed 3D structures within cellulose fibers. Furthermore; Cx43-Cx26 interaction and cell viability were investigated in stable HaCaT cells. Western blot results showed that increase in Cx26 protein, wild type or mutant, caused an increase in Cx43 levels. According to MTT assay, increase of wild type or D50Y mutant Cx26 did not change cell viability. Overall with these findings, provides a new point of view for KID syndrome mechanism and treatment.

ÖZET

ÜÇ BOYUTLU ORGANOTİPİK KİD SENDROMU DERİ MODELİ OLUŞTURULMASI VE KARAKTERİZASYONU

Keratitis, iktiyoz, sağırlık (KID) sendromu, connexin 26 gen mutasyonunun neden olduğu nadir bir genetik bozukluk olup, hastalarda oldukça zayıflatıcı ve korkunç etkiler gösterir. Sendromun kendisi karmaşıktır ve 2D kültür yöntemleri KID sendromunu araştırmak için karmaşık ve gerçek koşullara yakın olmamaktadır. Amacımız KID sendromu için organotipik 3D epidermis modeli oluşturmaktır. Her şeyden önce, yabani tip ve D50Y mutant Cx26 proteini ifade eden HaCaT kararlı hücre hatları üretildi. Yaptığımız immüno boyama, Western ve qRT-PCR sonuçları, bu hücre hatlarının KID cilt modeli oluşturmak için kullanılabileceği anlamına gelen Cx26 ifadesini doğrulamıştır. Organotipik KID sendromu cilt modeli yapımında ticari olarak temin edilebilen transweller kullanılmıştır. Model yapımı için önce fibroblast-kollajen karışımının transwellere koyuldu ve ardından oluşturulan hücre hatları karışımın üzerine aktarıldı. Sonra imuno boyama, üretilen cilt yapıları üzerinde gerçekleştirildi. Cytokeratin 14 boyama sonuçları, 3D modelin bazal tabaka epidermisine sahip olduğunu teyit etti. Ayrıca, KID cilt modeli, whatman kağıdı ile transwell yapısına bir alternatif olarak denendi. Phalloidin boyama sonuçları, üretilen hücre hatlarının selüloz lifleri yardımıyla 3D yapılar oluşturduğunu gösterdi. Ayrıca, Cx43-Cx26 etkileşimi ve hücre canlılığı araştırıldı. Western blot sonuçları, Cx26 protein yabani türünün veya mutantının artışının Cx43 seviyelerinde artışa neden olduğunu gösterdi. MTT analizlerine göre, vahşi tipli veya D50Y mutant Cx26'nın artışı hücre yaşayabilirliğini değiştirmedi. Bütün bu sonuçların ışığında, yaptığımız çalışma KID sendromunun mekanizmasını anlamak ve tedavisi için yeni bir bakış açısı sağlamıştır.

TABLE OF CONTENTS

LIST OF FIGURES viii

LIST OF TABLES ix

CHAPTER 1. INTRODUCTION 1

1.1. Gap Junctions 1
1.2. Connexins 2
1.3. Connexin Linked Human Diseases 4
1.4. Mechanisms of Connexin Mutations Related with Human Disorders 5
1.5. Connexin 26 and Human Diseases 8
1.6. Keratitis, ichthyosis, deafness (KID) syndrome 10

CHAPTER 2. MATERIALS AND METHODS 13

2.1. Propagation of HaCaT, NIH3T3 and 293T Cell Lines 13
2.2. Virus Production 13
2.3. Virus Titration 14
2.4. Infection and Generation of Stable HaCaT Cell Lines 15
2.5. Immunostaining and Fluorescence Imaging 16
2.6. Western blot 17
2.7. Quantitative RT-PCR Analysis 19
2.8. MTT Assay 21
2.9. Organotypic Culture of HaCaT Cell lines 21
2.10. Three Dimensional (3D) Cell Culture via Whatman Paper 22

CHAPTER 3. RESULTS AND DISCUSSIONS 23

3.1. Virus Titration 23
3.2. Infection and Generation of Stable Cell Lines 23
3.3. Cx26 Expression at Generated Cell Lines 25
3.4. Cx43 Expression changes in Generated Cell Lines 28
3.5. Immunostaining of Epidermal Differentiation Markers 30

3.6. Cell Viability Assay 33
3.7. Organotypic Culture of HaCaT Cell Lines with Transwell Inserts 34
3.8. Three Dimensional (3D) Cell Culture via Whatman Paper 36

CHAPTER 4. CONCLUSION 41

REFERENCES 43

LIST OF THE FIGURES

Figure **Page**

Figure 1. Graphic illustration of gap junctions.. 2
Figure 2. Connexin configurations forming various types of channels. 3
Figure 3. Classification of connexin loss of function mutations.. 6
Figure 4. Classification of connexin gain of function mutations.. 8
Figure 5. Illustration of each amino acid in Cx26 protein and deafness associated mutations.. 9
Figure 6. Microscope images of generated stable cell lines. 24
Figure 7. Determination of Cx26 localization and expression in stable HaCaT cell lines..... 25
Figure 8. Determination of Cx26 localization and expression in untransfected HaCaT cells..... 26
Figure 9. Comparison of Cx26 protein levels in stable HaCaT cell lines. 27
Figure 10. Cx26 mRNA expression levels of HaCaT cells lines..... 27
Figure 11. Determination of Cx43 localization and expression in stable HaCaT cell lines.. 28
Figure 12. Comparison of Cx43 protein levels in stable HaCaT cell lines. 29
Figure 13. Cx43 mRNA expression levels of HaCaT cells lines..... 30
Figure 14. Demonstration of differentiation marker Cytokeratin 14 in stable HaCaT cell lines..... 31
Figure 15. Demonstration of differentiation marker Cytokeratin 10 in stable HaCaT cell lines..... 32
Figure 16. Demonstration of differentiation marker involucrin in stable HaCaT cell lines..... 32
Figure 17. Demonstration of differentiation markers at untransfected HaCaT cells.. 33
Figure 18. Cell viability results of generated cell lines via MTT assay 34
Figure 19. Detection of Cx26 localization and expression in skin constructs. 35
Figure 20. Detection of cytokeratin 14 localization and expression in skin constructs.. 36
Figure 21. Visualization of HaCaT cell lines via phalloidin and DAPI staining..... 37
Figure 22. High magnification of phalloidin immunostaining. 37

Figure 23. Differentiation evaluation of HaCaT cell lines via cytokeratin 14 staining.. 38
Figure 24. Differentiation evaluation of HaCaT cell lines via cytokeratin 10 staining.. 39
Figure 25. Differentiation evaluation of HaCaT cell lines via involucrin staining.. 40

LIST OF TABLES

Table **Page**

Table 1. List of primary and secondary antibodies for immunostaining studies. 17

Tablo 2. List of primary and secondary antibodies used in Western blot. 19

Tablo 3. List of primer sequences used in qRT-PCR. 20

Tablo 4. Colony Count of Titration Assay. 23

CHAPTER 1

INTRODUCTION

1.1. Gap Junctions

Cells in a multicellular organism must be in coordination with other cells to properly function. This coordination is provided by direct cell contact and/or long ranged neural and endocrine signaling. Direct cell to cell interaction can be achieved by different means; one of such mean is mediated by gap junctions. Gap junctions are formed by hemichannel (connexon) of adjacent cells (Figure 1). They are membrane protein complexes that enable passage of small molecules from one cell cytoplasm to another [1]. Connexons can also stay as non-junctional hemichannels and facilitate molecule transfer between the cytoplasm and the extracellular environment [2]. This passage is driven by passive diffusion and selectivity of gap junctions depend on connexins that contribute to the formation of gap junction [3]. Gap junctions pore size is around 1.2 nm in diameter and molecules smaller than 1000 Da can pass freely [4] which can include second messengers [5] and siRNAs [6].

Several different gated transmembrane channels present in nature, each specialized for a different function. Three different families of channel forming proteins show similarity with connexins. These are innexins, pannexins and calcium homeostasis modulators [5]. All four of them share similar topology; one intra and two extracellular loops, four transmembrane domains, intracellular carboxy and amino terminus [5] and conserved three cysteine residues on the two extracellular loops (Figure 1c) [3]. Gap junctions are found in many phyla from metazoan to chordates [5]. In vertebrates' connexins form intracellular channels whereas in invertebrates, analogs are called innexins [7].

Gap junction facilitated intercellular communication is essential for tissue homeostasis, development, differentiation and apoptosis [8]. Passage of molecules provided by connexon between the cell cytoplasm and the extracellular environment also contributes homeostasis and cell synchronization [9].

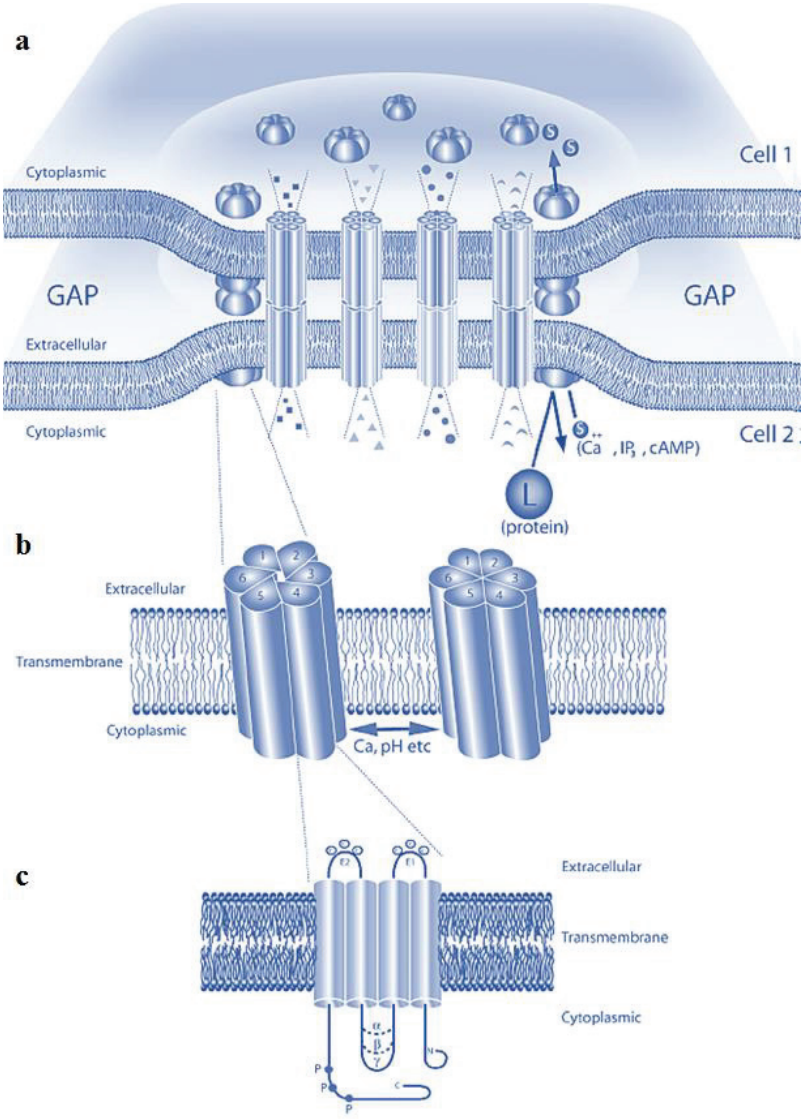

Figure 1. Graphic illustration of gap junctions**.** a. Two connexons dock each other to form gap junction and multiple channels clustering in a membrane location forms gap junction plaques. b. Connexons can be open or closed state according to various stimuli. c. Connexin protein is composed of cytoplasmic amino and carboxy terminus, four transmembrane alpha helix domain, one intra and two extracellular loops [10].

1.2. Connexins

Connexins are principal membrane protein of connexons. Each connexon is composed of six connexin subunits which form a hexameric structure and can dock to connexon of neighboring cells to form gap junction channel [11]. Multiple channels can cluster in a membrane location and form semi-crystalline structure resulting in gap

junction plaques (Figure 1a) [12]. Variety of connexin configurations is possible in the body since an individual cell can express more than one isoform. In a cell, connexons can be homomeric, composed of one type of connexin or heteromeric, composed of different connexins. In addition to that gap junctions formed from connexons between different cells can be homotypic, formed by identical connexons or heterotypic, formed by different connexons. These connexin configurations variety provide huge diversity in terms of functional capabilities in different cells and tissues (Figure 2) [13, 14].

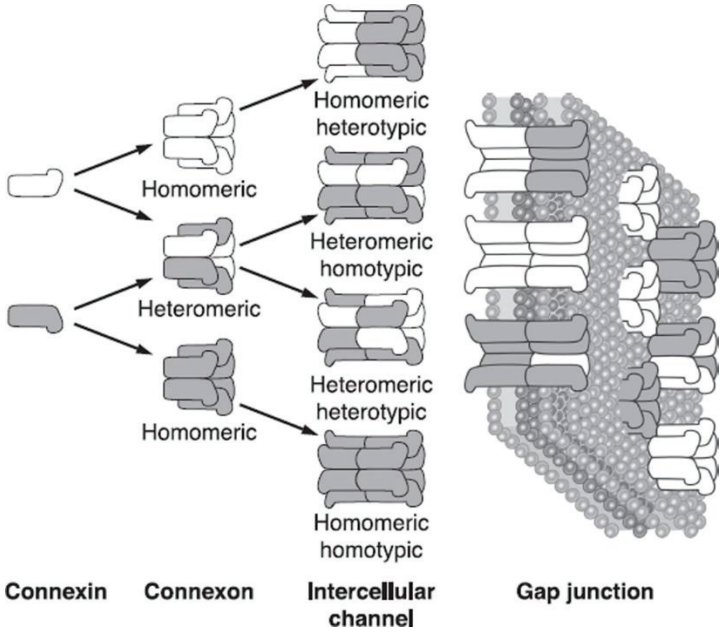

Figure 2. Connexin configurations forming various types of channels [15].

As a protein family, connexins have 21 members in the human genome [16]. Human connexins are classified into five families based on phylogenetic origins; alpha, beta, gamma, delta and epsilon [17]. There are two types of nomenclatures for connexins; the first nomenclature uses theoretical molecular mass or projected molecular size in kDa and species name such as mCx43 (Gja1) meaning mouse 43 kDa connexin protein [18]. In contrast, the second system divides connexins into subgroups according to their sequence similarity and length of the cytoplasmic domains [1]. This nomenclature abbreviates connexins with "Gj" which refers to gap junction and indicates discovery order with the serial number. For instance, Gja1 (mCx43) is the first discovered connexin in α-group [19].

Connexin molecules share similar topologic structure [4]. They are composed of cytoplasm facing amino and carboxy terminus, four transmembrane alpha helix domain, one intra and two extracellular loop structure [4]. Amino terminus domain is associated with voltage gating [20], carboxy terminus plays role in protein-protein interaction [21], alpha helix domains form the channel inside the cell membrane [22], intracellular loop regulates hemichannel acidification with carboxy terminus [21] and two extracellular loop structure play a part in hemichannel docking (Figure 1c) [23].

1.3. Connexin Linked Human Diseases

From aforementioned protein families; namely connexins, innexins, pannexins and calcium homeostasis modulators; only connexins are associated with inheritable diseases. First such discovery linked Charcot-Marie-Tooth disease (CMTX) to Cx32 [24]. Connexin mutations can result in various diseases such as common non-syndromic sensorineural deafness [25] and rarely observed oculodentodigital dysplasia (ODDD) [26] by affecting several different molecular mechanisms such as defects in connexin assembly, failures in quality control, aberrant trafficking and abnormal gating properties [27].

Gap junctions are crucial for cochlear physiology. Inside of inner ear, both supporting cells and connective tissue network form gap junction with overwhelmingly Cx26 and Cx30 [28]. The most common inherited disease resulting from connexin linked mutation is a non-syndromic sensorineural hearing loss. For example, almost 50 % of autosomal recessive non-syndromic hearing loss cases are associated with over 200 different Cx26 mutations [29].

In their life cycle keratinocytes differentiate into stratum basale, spinosum, granulosum and corneum [30]. During their life cycle, eight different connexins are expressed in a specific pattern [30]. For instance, Cx26, Cx30, Cx30.3, Cx31, Cx31.1, Cx40, Cx43 and Cx45, are all expressed in spinosum and to some degree in granulosum [31]. Number of different mutations in connexin genes can manifest themselves as various skin diseases and abnormalities such as Clouston syndrome, Bart-Pumphrey syndrome, erythrokeratodermia variabilis (EKV), Vohwinkel syndrome and keratitis, ichthyosis, deafness (KID) syndrome [32].

Connexins also have a function in myelination. Cx32 and Cx47 have been linked to CMTX and Pelizaeus-Merzbacher-like disease, respectively [33]. Further, Cx43 is linked to ODDD [26]. Gap junction homeostasis is vital for all types of tissue but it is especially true for avascular tissues such as lenses where cells are dependent on gap junctions for nutrient and waste transport [15]. Almost 25% of non-syndromic hereditary cataracts caused by Cx46 and Cx50 mutations [34]. Different connexins such as Cx40, Cx43 and Cx45 are expressed in different areas of the heart [35]. Cx40 mutations linked to atrial fibrillation (AF) and Cx43 mutation associated with sudden infant death syndrome (SIDS) and AF [36].

1.4. Mechanisms of Connexin Mutations Related with Human Disorders

Several different mutations can occur in connexin genes, leading to hereditary disorders via several mechanisms. These mechanisms are classified into two broad groups; loss of function and gain of function. Mutations that ultimately result in reduced or complete loss of normal function are classified as loss of function mutation. The gain of function mutations alters the gene in a way that the resulting gene gain new features and/or functions. Both losses of function and gain of function mutations can be further classified into several sub-mechanisms. Subgroups of loss of function mutation mechanisms are (1) truncation defects, (2) trafficking and misfolding defects, (3) interactome defects, (4) docking defects and (5) permeability and gating defects (Figure 3) [37].

Truncation defects can be a result of several mutations such as nonsense or frameshift mutations. Such mutations can cause short or long truncation and either knock-out the connexin in short truncation case or loss of some function in long truncation case. For example, a Cx26 mutation (167delT) seen in the Ashkenazi Jewish population causes a shift in the open reading frame resulting in a truncation because of the addition of a stop codon after 25 amino acid and cause non-syndromic recessive deafness [38].

Trafficking defects, on the other hand, caused by mutations that trap connexin molecules in intracellular compartments mostly in the endoplasmic reticulum (ER), ER-Golgi intermediate and Golgi apparatus. This retention may cause premature

degradation and put cells under stress [39]. As an example, cataract responsible mutation Cx46fs380 result in polypeptide extension. This extension caused by the mutation contains a motif that change trafficking of Cx46 and thus result in the accumulation in the ER-Golgi intermediate [40].

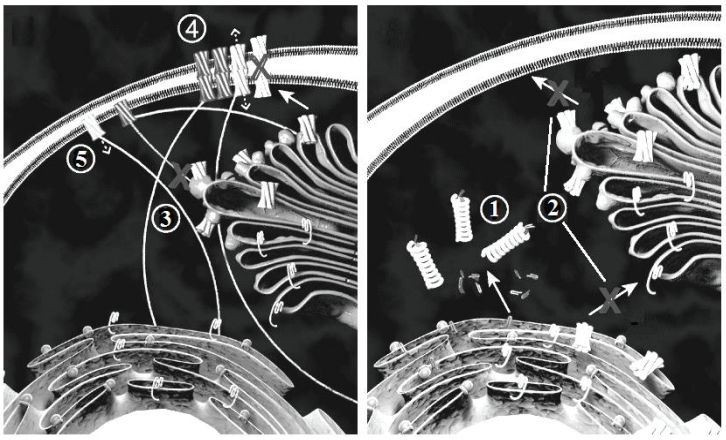

Figure 3. Classification of connexin loss of function mutations. 1; truncation defects, 2; trafficking and misfolding defects, 3; interactome defects, 4; docking defects 5; permeability and gating defects [37].

Except connexin themselves, connexin mutations influence interactome partners thus also have consequences in connexin function and biogenesis. Several connexin interactome partners have been identified and these interactions can affect connexin trafficking, post-translational modification, stabilization and function [2]. For instance, ERp29 (quality control chaperone) binds to the second extracellular loop of Cx43 and delays oligomerization until Cx43 reaches Trans Golgi Network [41]. Thus, secondary extracellular loop mutation of Cx43 such as H194P and S201F/Y were thought to change Cx43-chaperon interaction and may cause premature oligomerization or misfolding [42].

As stated before; two connexons from neighboring cells dock to form gap junctions. This docking requires minimum four hydrogen bonds between the second extracellular loop interfaces [43]. For example, an asparagine residue at extracellular loop 2 in Cx32 is crucial for heterotypic docking between Cx32 and Cx26 and when

mutated to tyrosine, Cx32 forms connexons but not the gap junction with either Cx26 or Cx32 [44].

The last type of loss of function mutation defects is permeability and gating defects. The problem with these types of mutation is not related to trafficking or assembly characteristic of connexins but related to reduced ion and molecule permeability of formed connexons and gap junctions [45]. Cataract related Cx46 mutations, D3Y for example, can form gap junction plaques indicating that it has no problem with trafficking or junction formation. However, voltage-clamp experiments on *Xenopus* oocyte showed that oocyte pairs with Cx46D3Y mutation failed to form gap junctional coupling in contrast to wild type Cx46. This indicates reduced gating properties and altered charge selectivity [46].

The gain of function mutations, on the other hand, are mutations that alter the gene in such manner that the resulting gene gain new features and/or functions. Subgroups of gain of function mutations are (1) enhanced connexon permeability, (2) gain of interactome partners, (3) changes at connexin half-life, and (4) enhanced junction permeability (Figure 4) [37].

The first type of gain of function mutation is enhanced connexon permeability, in other words, formation of leaky hemichannels. In general, connexons are thought to be closed *in vivo* and they open when appropriate stimuli are present [47]. Some mutations can hamper this opening mechanism in such a way that connexon leaks, opens when it should not or stay open. A good example of such mutation is KID syndrome mutant Cx26A40V. It is proposed that Cx26A40V cause enhanced connexon activity, leaky connexons via change in gating properties and decreased regulation by Ca^{2+} concentration [48].

Similar to loss of function mutations, some gain of function mutations are related to connexin interactome. In these mutations, connexins gain ability to bind some proteins or other connexin members that they generally do not interact with [37]. Cx43Fs260 frame shift mutation cause ODDD. Organotypic culture studies of rat epidermal keratinocytes showed that fs260-expression lowers levels of Cx43, Cx26 and loricrin when compared to wild-type Cx43 expression. So possible interactions with co-expressed connexins in keratinocytes lead to various skin problems that accompany ODDD [49].

The half-life of a protein in the cell is one of the main parameters at its regulation. Therefore, mutations that change half-life of connexin molecules have a

variety of consequences. Cx43G138R and G143S mutations associated with ODDD, for example, have longer half-life thanks to delayed cell surface internalization [50]. Opposite to that, Cx40G38D and V85I have shorter than normal half-life because of rapid degradation by the proteasome and are linked to AF [51].

Finally; some gain of function mutations has been demonstrated to cause an enhanced gap junction permeability. EKV causing Cx31G12R mutant shows increased connexon activity and dye coupling than WT Cx31. Proposed mechanism for this increase is deficient channel closing that presumably related to impaired ability of amino terminus to close the pore [52]. In contrary, there are also studies suggesting that Cx31G12R mutation has defects at both trafficking and junction assembly [53, 54]. So further studies needed to uncover enhanced gap junction permeability gain of function mutation.

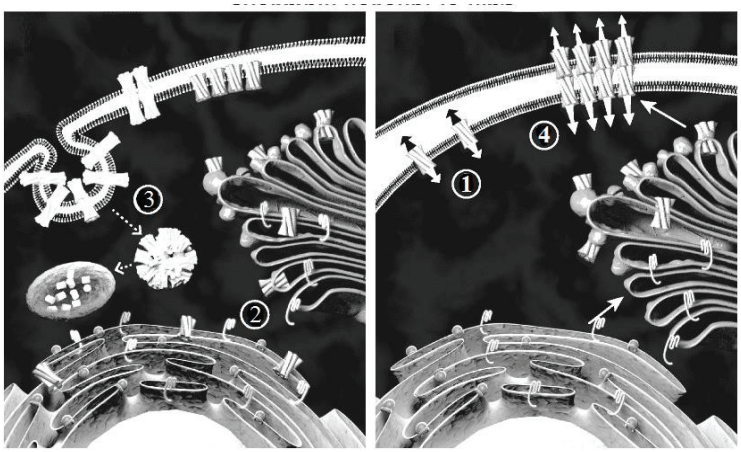

Figure 4. Classification of connexin gain of function mutations. 1; enhanced connexon permeability, 2; gain of interactome agents, 3; changes at connexin half-life, 4; enhanced junction permeability [37].

1.5. Connexin 26 and Human Diseases

Connexin 26 (Cx26) protein is encoded by Human Gap Junction Beta 2 (GJB2) gene (GenBank M86849, OMIM: * 121011) which is located at 13q11-q12 chromosomal location. The coding region of GJB2 gene consists of 680 base pairs that are made of two exons [55]. Cx26 is a beta class gap junction protein and with 26 kDa

molecular size it is the smallest human connexin isoform. It is primarily expressed in the cochlea, the epidermis and the cornea [56].

As mentioned above, connexins form gap junctions to facilitate cell-to-cell and cell-to-extracellular environment small molecule transportation. The cochlea is one of the most complex organ and many genes play role in its proper functioning so mutations in these genes can cause hearing loss [57]. About 2 children in 1000 have hearing loss [58] and in 50% of the cases, the underlying reason is genetic [59].

In the cochlea, Cx26 expression is seen in stria vascularis, supporting cells, spiral ligament and spiral limbus [55]. Potassium recycling in the cochlea is essential for sensorineural hearing function and this recycling only possible with transport function of normal Cx26 [60]. Gap junctions regulate ion exchange between cochlear cells and therefore provide the necessary structure for potassium recycling [61].

Hearing loss can be divided into nonsyndromic hearing loss and syndromic hearing loss. Because of its essential function in cochlea, Cx26 mutations have been related to both nonsyndromic and syndromic hearing loss (Figure 5) [57].

GJB2 gene has several identified variants in different populations. These variants are result of missense, nonsense, insertion, deletion and frameshift mutations. Interestingly, despite genetic heterogeneity of hearing loss, GJB2 gene variations are responsible for 50% of the nonsyndromic hearing loss cases [57, 62]. GJB2 gene mutations are also responsible for syndromic forms of hearing loss such as Bart-Pumphrey syndrome [63], Vohwinkel syndrome [64] and KID syndrome [65].

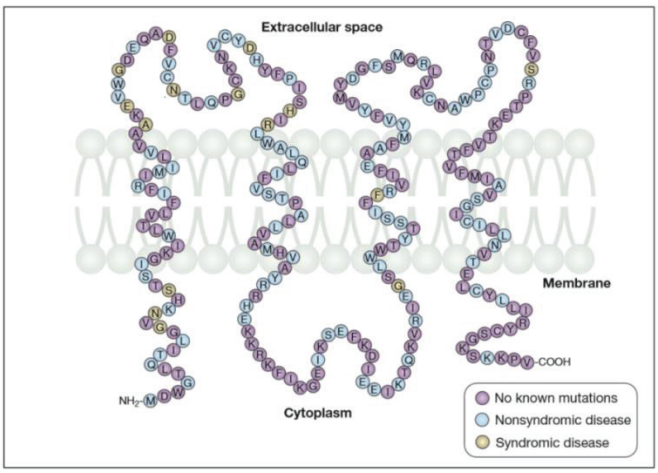

Figure 5. Illustration of each amino acid in Cx26 protein and deafness associated mutations. Blue amino acids indicate nonsyndromic disease. Yellow amino acids indicate syndromic disease [66].

1.6. Keratitis, ichthyosis, deafness (KID) syndrome

KID syndrome is named after its clinical traits; keratitis, ichthyosis and deafness. First documented case was reported by Burns in 1915 [67]. Syndrome itself was recognized as a distinct case in 1981 by Skinner et al [68]. KID syndrome is a rare disease, just about 100 cases have been reported around the world [69]. Syndrome itself is extremely debilitating and hard to treat. Early diagnosis is crucial as well as non-stop management because of skin superinfection and benign tumors with the ability to turn into malignant [70].

KID syndrome has variety of clinical features. Syndrome mainly affects the skin, the cornea and the cochlea. As skin complications go, it can manifest as hyperkeratosis or erythroderma at neonatal period [71]. KID syndrome may also cause generalized alopecia and verrucous hyperkeratosis, orangish reticulated plaques and stippled palmoplantar keratoderma [69, 72]. Cyst formation can also occur [70] and some studies associate syndrome with follicular occlusion [73, 74].

Except skin complications, hearing loss and ocular impairments accompany KID syndrome. Hearing loss is seen in almost all cases and is usually non-progressive and congenital. Because of congenital hearing loss, patients often suffer from speech impairment [69]. Ocular anomalies include keratoconjunctivitis sicca, neovascularizing keratitis, corneal epithelial defects, limbal defects and photophobia. These anomalies show variety in terms of severity and age of onset [75].

Overall, KID syndrome is an unpredictable disease. Manifestation can differ from patient to patient, skin complication are usually neonatal but can onset at adulthood and the cutaneous lesion is also unpredictable [76]. Ocular anomalies show variety and patients are at high risk of malignant tumors [77]. Superinfections are also common and nearly half of the patients [78] have some type of chronic infection caused by bacterial [79] or fungal agents [80].

The main mutation that linked to KID syndrome is GJB2 gene mutations. As mentioned before, GJB2 gene encodes Cx26 protein. The syndrome is usually sporadic but there are cases of familial cohorts [81, 82]. Like heterogeneity in symptoms of KID syndrome, its inheritance also varies. It is inherited via autosomal dominant manner but there are also autosomal recessive cases [83]. There are several Cx26 mutations such as A40V, G12R, G45E and D50Y that result in KID syndrome [48, 84]. Between those

mutations, D50N is the leading GJB2 mutation causing KID syndrome [70]. G45E and A40V mutations are responsible for enhanced connexon activity and this enhanced activity ultimately leads to cell death [85]. Further, G12R, D50Y and I30N mutations also cause formation of aberrant connexons [86, 87]. Aberrant connexons can alter permeability of channel and cause increased Ca^{2+} concentration in cell and ATP leak from the cell [88, 89].

Up to date, two mouse models for KID syndrome have been reported and in both models, mutations result in the formation of aberrant connexons [90, 91] . Work on Cx26S17F mouse model showed that mutation was survivable only in heterozygous mice and lethal for homozygous mice. Mutant protein forms aberrant connexons and this causes hyperplasia of tail and hearing loss [90]. Another study on Cx26G45E mouse model indicates that mutant mice had lower vitality and demonstrated abnormalities similar to KID syndrome patients such as hyperkeratosis, scaling in skin, hyperplasia and acanthosis [91]. Limitation of mouse models includes; high cost, development time and high variability of disease onset and progression [92]. Also connexin expression in mice skin differs from human skin [91]. These limitations direct us towards to human skin constructs. There are number of skin constructs developed and they are usually formed by keratinocytes that differentiated at air-liquid surface of pseudo dermis [93]. Skin constructs can be grouped into three categories; models with only epidermal components, models with dermal components and models that contain both epidermal and dermal components [94]. It is shown that fibroblasts influence keratinocytes to make basal proteins and takes role in keratinocyte proliferation, epidermal layer development [95]. So skin model that includes both dermal and epidermal layer will be closer to real conditions and will help us to solve complex processes that are not possible with mono layered two dimensional models.

As mentioned before, skin complications are main clinical features of KID syndrome. Skin is the largest protection organ in the body. It composes of three distinct layers; epidermis, dermis and hypodermis. The epidermis is the outer layer of the skin and formed by keratinocytes. The dermis is located between epidermis and hypodermis and composes of extracellular matrix and fibroblasts. The deepest layer of the skin is hypodermis and includes fibroblasts as well as adipocytes [96]. Keratinocytes in the epidermis form protective barrier by their differentiation. During their life cycle, keratinocytes migrate towards the surface of skin and as they pass spinosum and granulosum, Ca^{2+} permeability increases. This change causes filaggrin to aggregate with

other materials and cells die to form the protective shields [97]. This differentiation process depends on several mechanisms including cellular communication provided by gap junctions. During differentiation process, several connexin proteins such as Cx26, Cx43, Cx30, Cx31 and Cx30.3 are expressed and their expressions have a distinct pattern in the epidermis. Cx26 expression is seen in the palmoplantar epidermis, all interfollicular cells have Cx43 expression, and differentiated epidermal cells shows Cx30, Cx31 and Cx30.3 expression [56].

1.9. Aim of the Study

KID syndrome is a complex disorder with fluid symptoms and limited number of cases. Lack of differentiation process and one layer structure of the two dimensional models are not enough to understand processes ongoing at KID syndrome. More complex and close to real physiological conditions are needed for such complex syndrome with various symptoms. So the generation of a three dimensional organotypic KID syndrome model will help us to overcome those limitations. For this purpose, Cx26 mutation and WT Cx26 containing cells will be used to generate three dimensional organotypic KID syndrome skin model. By comparison of D50Y mutant with the WT Cx26, cellular processes that lead to KID syndrome and effects of aberrant connexons on epidermal organization and differentiation will be uncovered.

CHAPTER 2

MATERIALS AND METHODS

2.1. Propagation of HaCaT, NIH3T3 and 293T Cell Lines

HaCaT, NIH3T3 and 293T cells were used in experiments. High glucose Dulbecco's Modified Eagle Medium (DMEM) (GIBCO, Cat# 41966-029), 10% Fetal Bovine Serum (FBS) (Biological Industries, Cat# SH30243.01) and 1% penicillin streptomycin (Invitrogen, Cat# 1092595) mixture was filtered and used to grow HaCaT and 293T cell lines. During experiments, HaCaT cells were used to generate stable cell lines containing WT and D50Y Cx26 mutation. It is shown that Cx26D50Y mutation increases internal Ca+2 ion concentration in the cell by forming leaky hemichannels [87]. So to prevent cell death, additional Ca^{+2} ions were provided to the cells during propagation of stable HaCaT cell lines. 0.34 µl 1 M Ca^{+2} solution was added per ml of DMEM. HaCaT and 293T cells were grown in tissue culture treated plates. In order to lift HaCaT cells from plates, cells were incubated with EDTA (BI, Cat# 03-015-1B) for 20 minutes then EDTA was removed and 0.05% Trypsin/EDTA (BI, Cat# 03-053-1B) added. Cells were incubated with trypsin solution for 10 minutes. For 293T cells, EDTA incubation step was skipped. Both cell lines were grown at 5% CO_2 and 37^{o}C condition inside of an incubator.

NIH3T3 cells were grown in filtered high glucose DMEM, 10% Newborn Calf Serum (NBCS) (Life Technologies, Cat# 16010159) and 1% penicillin streptomycin mixture. Tissue culture treated plates were used for NIH3T3 cells and lifting was performed 10 minutes incubation with 0.05% Trypsin/EDTA similar to 293T cells. Cells were grown at 5% CO_2 and 37^{o}C condition.

2.2. Virus Production

The 293T cells (4-5x10^{6}) were plated onto 10 cm plates and incubated 24 hours before transfection. At transfection day, plasmid DNAs were vortexed and quickly spun. A total of 3 different plasmids was used; MSCV2.2 (empty), Cx26WT (contains

wild type connexin 26) and Cx26D50Y (contains D50Y mutation in Cx26 gene). Fugene HD (Promega Cat# E2311) mixture was prepared in serum free medium to the final volume of 500 µl. 3 different Fugene HD mixture was prepared with 2 µg of retroviral plasmid, 2 µg of packaging vector (Pcl10A) and 12 µl of Fugene HD. The mixture was pipetted into medium. After 30 minutes of incubation at room temperature, mixture was added into 10 cm plates containing 293T cells in drop by drop fashion and mixture was spread evenly through plate.

After another 24 hours incubation in the incubator (37^{o}C, 5% CO_2), medium was aspirated. Then 8.5 ml of fresh medium was added gently in each plate and plates were placed in the incubator.

After 48 hours from transfection, first virus collection was performed. Virus containing mediums were collected into 50 ml falcon tubes. Cap of the falcon tube was sealed with parafilm and stored at 4^{o}C. 8.5 ml fresh medium was added gently onto the plates and plates were left for incubation. Second virus collection performed after 24 hours from the first one. Virus containing mediums were collected into the previous collection. Virus collections were aliquoted into falcon tubes, sealed with parafilm and stored at -80^{o}C until usage. In the end, 3 different virus types were collected; MSCV, Cx26WT and Cx26D50Y. This procedure was performed three different times so three generation of viruses were prepared.

2.3. Virus Titration

NIH3T3 cells ($2x10^5$) were plated into 6-well plates for each virus type (MSCV, Cx26WT and Cx26D50Y) a day before infection. Polybrene mixture was prepared with medium and polybrene stock solution (8mg/ml) to get 8 µg/ml final concentration. Wells were labeled as 0, 10^{-3}, 10^{-4} and 10^{-5}. Virus dilutions were prepared as follows; 100µl stock virus solution was added into 900µl Polybrene-medium mixture to get 10^{-1} dilution. Then, 100µl 10^{-1} virus dilution was mixed with 900µl Polybrene-medium mixture to get 10^{-2} dilution. 10^{-3}, 10^{-4} and 10^{-5} virus dilutions were prepared in similar fashion. After dilutions were completed, media of the wells were aspirated. To the appropriately labeled wells, 1 ml virus dilutions (10^{-3}, 10^{-4} and 10^{-5}) were added. As a mock control, 1 ml polybrene-medium mixture was added into 0 labeled well. Then plates were put in incubator (37 ^{o}C, 5 % CO_2).

After 1 day of incubation, virus removal was performed via aspirating virus containing medium from each well and replacing with a 2 ml fresh medium.

After 2 days, the selection was performed. Antibiotic containing medium with puromycin to a final concentration of 2 μg/ml was prepared. Cells were trypsinized from 6-well and placed in 10 cm plates containing antibiotic medium. Antibiotic medium was changed twice a week according to number of floating dead cells. The selection was continued until all cells in the mock control plate were dead.

Upon death of all cells in the mock plate, crystal violet staining was performed. First, 0.5% crystal violet solution was prepared with 1 g crystal violet and 200 ml 1X Phosphate Buffer Saline (PBS) (BI, Cat# 02-023-5A) at room temperature. Solution was filtered through filter paper to avoid precipitates. After that, plates were washed with PBS twice under the hood to remove all medium and floating dead cells. Then 4 ml of PBS was added into plates and plates were transferred to the bench. All the PBS was aspirated from plates and 4-6 ml 0.5% crystal violet solution was added onto plates. Plates were incubated in a shaker for 10 minutes at room temperature. After incubation, violet solution was removed and plates were rinsed with PBS. Then plates were incubated again with 4-6 ml PBS at shaker for 10 minutes at room temperature. After that, PBS was removed and plates were rinsed with PBS until mock plate become almost transparent. Plates were left on paper towels in inverted fashion for overnight. Finally, colony counting was performed for each plate and data was collected. Titration was performed after every virus generation.

2.4. Infection and Generation of Stable HaCaT Cell Lines

Before the infection, $4x10^5$ HaCaT cells per well were plated onto 6-wells for each virus type. Wells were labeled as MSCV, Cx26WT and Cx26D50Y. Viruses were prepared according to the result of virus titration assay. Polybrene was added to viruses as final concentration of 8 μg/ml. After that, medium of the cells was aspirated. To the appropriately labeled wells, 2 ml viruses (MSCV, Cx26WT and Cx26D50Y) were added. Again as a mock control, 2 ml polybrene-medium mixture was used and added into control labeled well. Then, cells were incubated.

After 1 day of incubation, viruses were removed via aspirating medium and 2 ml fresh medium was provided. After 2 days, the selection was started. Medium containing

2 μg/ml promycin was prepared. Cells were replated into 10 cm plates containing antibiotic medium. After that, antibiotic medium was replaced twice a week. The selection was finished when all cells in mock plate were dead. In the end, three stable HaCaT cell lines (MSCV, Cx26WT and Cx26D50Y) were generated. Generation of stable cell lines was performed three times.

2.5. Immunostaining and Fluorescence Imaging

Infected stable HaCaT ($4x10^5$) cells were plated on coverslips and incubated for 24 hours in incubator (37 ^oC, 5 % CO_2). The first medium was aspirated and then cells were washed two times with 1 ml PBS. Cells were fixed with 4% paraformaldehyde (PFA) at room temperature for 20 minutes. After that, cells were washed for three times with PBS and cells were permeabilized with 1 ml 0.1% Triton X-100/ PBS at room temperature for 15 minutes. After permeabilization, cells were blocked with 1 ml 3% bovine serum albumin (BSA) in 0.1% Triton X-100/ PBS for 30 minutes while shaking at 60 rpm at room temperature. During blocking, primary antibody dilutions were prepared with 3% bovine serum albumin (BSA) in 0.1% Triton X-100/ PBS. After that, cells were incubated with 500 μl diluted primary antibody for 60 minutes at room temperature or overnight at 4^oC. Then cells were washed with 1 ml PBS for three times with 10 minutes intervals. Secondary antibody dilution was prepared again with 3% bovine serum albumin (BSA) in 0.1% Triton X-100/ PBS and DAPI (1:200) (Sigma, Cat# D95242-10MG). Cells were incubated with secondary antibody dilution for 60 minutes at room temperature. After that cells were washed again with PBS for three times with 10 minutes intervals. Coverslip was dipped in ddH_2O and briefly dried. Then coverslip was mounted on 15-30 μl Ibidi mounting medium (Ibidi, Cat# 50001) and edges of coverslip were stabilized with transparent nail polish to prevent drying. Fluorescence microscope (IX83 Olympus, Japan) was used for imaging and cellSens (Olympus) and ImageJ (NIH) softwares were used for merging images. Several immunostaining experiments were performed with primary and secondary antibodies listed in Table 1.

For phalloidin staining, the protocol at above was followed with small differences. Instead of incubation with primary and secondary antibodies, one incubation step was performed. This incubation was done with mixture of 3% BSA in

0.1% Triton X-100/ PBS, DAPI (1:200) and phalloidin (1:200) (Invitrogen Ca#A12370).

Table 1. List of primary and secondary antibodies for immunostaining studies**.**

Antibody	**Catalog Number**	**Dilution Factor**
Rabbit anti-Connexin 26	Invitrogen Cat# 71-0500	1:500
Rabbit anti-Connexin 43	Invitrogen Cat# 71-0700	1:500
Mouse anti-Involucrin	Abcam Cat#ab68	1:500
Mouse anti-Cytokeratin 10	Abcam Cat#ab9025	1:300
Mouse anti- Cytokeratin 14	Abcam Cat#ab7800	1:300
Alexa Flour 555 Goat anti-Rabbit IgG (H+L)	Invitrogen Cat# A21428	1:1000
Alexa Fluor 555 Rabbit Anti-Mouse IgG (H+L)	Invitrogen Cat# A21428	1:1000

2.6. Western blot

Stable HaCat cell lines ($4x10^5$ per well) were plated on a 6-well plate. After 24 hours in incubator (37^oC, 5 % CO_2), wells were washed with PBS three times. Plates were flash-frozen with liquid nitrogen after all liquid had been removed from wells.

First, working solution was prepared with 989 µl lysis buffer (Tris-HCl, Triton X 100), 10 µl protease inhibitor (Sigma, Cat# P8340) and 1 µl Dithiothreitol (DTT) (Sigma #Ca 43816). Cells were put on ice. Volume of 150 µl working solution was added per well. Then wells were scraped and lysates were collected in 1.5 ml Eppendorf tubes. After that, contents of tubes were homogenized via passing through insulin syringe 12 times. Lysates were left to incubate for 20 minutes on ice. After incubation,

tubes were vortexed and spun for 10 minutes at 4°C at 14,000 RPM. Finally, supernatants were collected and stored at 80°C.

Quantification of the protein isolate was done via Bradford assay. First protein standards were prepared by serial dilution from stock solution of BSA (Biolabs Ca#B9000S). Then 790 µl distilled H_2O, 200 µl Bradford reagent and 10 µl protein sample were mixed. For blank, just 10 µl distilled H_2O was used. Mixtures were added into cuvettes and absorbance measurements were performed at 595 nm via Genesys 10S VIS spectrophotometer (Thermo Scientific).

Bradford assay results were used to prepare 50 µg total protein for each sample. Then, samples were incubated for 5 minutes at 95°C with 5 µl 5X SDS loading buffer that contained 10% SDS, 30% Glycerol, 250 mM Tris-HCI, 5% β-mercaptoethanol, 0.02% Bromophenol Blue. During incubation, acrylamide gel was prepared. Gel consisted of two parts; resolving gel and stacking gel. First, 5 ml 15% resolving gel (distilled H_2O, 30% Acrylamide, 1M Tris pH 8.8, 10% SDS, 10% APS and TEMED) was prepared. Vertical gel line was generated with butanol. After resolving gel was polymerized, butanol was removed and 3 ml 5% stacking gel (distilled H_2O, 30% Acrylamide, 1M Tris pH 6.8, 10% SDS, 10% APS and TEMED) was added on top of the resolving gel. Stacking gel was left to polymerize with inserted comb. Then running buffer (192mM Glycine, 25mM Tris Base, 0.1% SDS) was added, the comb was removed and samples were loaded. Gel was run at 20mA for 3 hours. After that, gel was removed from its glass container and placed on a paper, nitrocellulose membrane was put on the gel. Then, they were placed in transfer equipment and transfer buffer (192 mM Glysine, 25 mM Tris Base, 20% methanol) was added. The transfer was performed at 250 mA for 2 hours, equipment was kept on ice to prevent heating.

After transfer, the nitrocellulose membrane was blocked with 5% powder milk for 2 hours at room temperature. Then, the membrane was incubated with primary antibody at room temperature for 2 hours or at 4°C overnight. After incubation with primary antibody, the membrane was washed with TBS-T (1X Tris-Buffered Saline and Tween 20) for 3 times with 5 minutes intervals. Then the membrane was incubated with secondary antibody at room temperature for 2 hours. After that, the membrane was washed again with TBS-T for 3 times with 5 minutes intervals. SuperSignal West Pico Chemiluminescent Substrate (Thermo, Cat# 34080) was utilized to visualize the

membrane with Fusion SL (Vilber). Western blot experiments were performed with the primary and secondary antibodies listed in Table 2

Tablo 2. List of primary and secondary antibodies used in Western blot.

Antibody	**Catalog Number**	**Dilution Factor**
Rabbit anti-Connexin 26	Invitrogen Cat# 71-0500	1:500
Rabbit anti-Connexin 43	Invitrogen Cat# 71-0700	1:500
Goat anti-Mouse immunoglobulins/HRP	Dako Ca# 00095437	1:1000
Goat anti-Rabbit immunoglobulins/HRP	Dako Ca# 00072118	1:2000

2.7. Quantitative RT-PCR Analysis

Similar to Western blot, stable HaCat cell lines ($4x10^5$ per well) were plated on a 6-well plate and incubated for 24 hours (37^oC, 5% CO_2). Then wells were washed with PBS three times, all liquid was removed and plates were flash-frozen with liquid nitrogen. Then cells were taken to bench for RNA isolation process.

For RNA isolation, RNA isolation kit (Invitrogen, Cat# AM1910) were used and manufacturer's protocol was followed. First, cells were put on ice and 300 µl lysis buffer containing 1% β-mercaptoethanol was added to each well. Then wells were scraped and contents were transferred into 1.5 ml RNAse-free Eppendorf tubes. Contents were homogenized with insulin syringe 12 times. 300 µl 70% ethanol was added to each tube and tubes were vortexed. Then the mixture was loaded into the column and centrifuged at 12,000 g for 15 seconds (Except elution step, all centrifugation steps were done at 12,000 g for 15 seconds). Flow through was removed and 350 µl wash buffer I was added. Again, tubes were centrifuged and flow through was removed. Columns were incubated with 80 µl DNAse working solution (Invitrogen, Cat# 18068-015) for 15 minutes at room temperature. After incubation, columns were washed again via 350 µl wash buffer I and centrifugation. Columns were

transferred to new reaction tube and washed twice with 500 µl wash buffer II and centrifugation. Another centrifugation was performed to dry columns. Finally, columns were transferred into recovery tubes and RNA elution was performed with 40 µl RNase-free H_2O via centrifugation for 2 minutes at 12,000 g. ND-1000 Spectrophotometer was used to measure quality and quantity of isolates.

cDNA production was done using Fermentas First Strand cDNA Synthesis Kit (Thermo, Cat# K1622). 1 µg/µl total RNA, 1 µl random primer and an appropriate amount of RNAse-free H_2O were mixed to get 12 µl total reaction volume. Then the mixture was incubated at 65^oC for 5 minutes. After incubation, master mix containing 4 µl reaction buffer, 2 µl dNTPs, 1 µl riboLock RNase inhibitor and 1 µl reverse transcriptase was added on top of RNA mixture. Applied Biosystems, Veriti Thermal Cycler was used to synthesize cDNA with the following program: 25^oC for 5 minutes, 42^oC for 1 hour and 70^oC for 5 minute incubation cycles.

Roche, LightCycler® 96 was utilized for SYBR Green based qRT-PCR. cDNA, primers (Table 3) and SYBR Green were mixed and loaded on 96-well plate. qRT-PCR program consisted of 98^oC for 5 minutes, cycles of 95^oC for 30 seconds and 60^oC for 30 seconds and 72°C for 10 minutes. GAPDH was used as housekeeping control and results were analyzed via LightCycler® 96 Software 1.1.

Tablo 3. List of primer sequences used in qRT-PCR.

Gene	**Forward Primer (5' to 3')**	**Reverse Primer (5' to 3')**
Human_Cx26	CTGCAGCTGATCTTCGTGTC	AAGCAGTCCACAGTGTTG
Human_Cx43	GTGCCTGAACTTGCCTTTTC	CCCTCCCAGCAGTTGAGTAGG
Human_GAPDH	GAAGGTGAAGGTCGGAGTCA	AATGAAGGGGTCATTGATGG
Human Keratin14	CCTCTCCTCCTCCCAGTTCT	GATCTTCCAGTGGGATCTGTGT
Human Keratin10	GCCAACATCCTGCTTCAGAT	GGCTCTCAATTTGCATCTCC

2.8. MTT Assay

MTT (3-(4,5-Dimethylthiazol-2-yl)-2,5-Diphenyltetrazolium Bromide) was used to detect cell viability differences between stable HaCaT lines. Cells (10^4 per well) were plated on 24-well plate. After 24 hours, MTT assay started. The protocol was performed in dark to reduce effects of light on MTT. First 10 % MTT solution was prepared via mixing MTT and DMEM. Then, normal medium in wells was aspirated and 600 µl 10% MTT solution was added to each well. Then, wells were put in incubator (37^oC, 5% CO_2) for 4 hours. After incubation, wells were treated with 600 µl DMSO (Dimethyl sulfoxide) and soft pipetting was performed to solubilize MTT crystals. Then absorbance was measured at 570, 650 and 670 nm with Thermo Scientific Multiskan Spectrum. MTT measurements were performed at days 1, 3 and 7.

2.9. Organotypic Culture of HaCaT Cell lines

Firstly, NIH3T3 cells were trypsinized and counted. Then cells were diluted or concentrated to get appropriate cell number in 100 µl suspension. Cell suspension was put on ice as well as other solutions and collagen. For 300 µl collagen solution; 44.33 µl 0.1 M NaOH, 30 µl 10X DMEM, 33 µl autoclaved H_2O and 192.7 µl 8.3 mg/ml collagen stock solution were mixed on ice. Then 100 µl NIH3T3 cell suspension containing $2x10^6$ NIH3T3 cells were mixed with collagen and 60 µl of final mixture (4 mg/ml collagen) was loaded into 0.3 µm pore size transwell inserts (Costar Ca#3470). Wells were left for 30 minutes in incubator (37^oC, 5% CO_2) for collagen polymerization. After polymerization, DMEM was added in wells until it covers all collagen surface. After 3 days of incubation, DMEM was removed from wells. Then 50 µl cell suspension containing $5x10^4$ stable HaCaT cells (MSCV, Cx26WT, Cx26D50Y) were added on collagen surface. After 30 minutes of waiting to let cells to attach surface, enough DMEM to cover collagen was added and cells were incubated for 3 days. Then, DMEM was carefully removed and cells were air-lifted. Cells were left in the incubator for 21 days and DMEM was refreshed every 3 days.

After 21 days at air-liquid surface, immunostaining and quantitative RT-PCR analysis were performed. For immunostaining, the procedure at Section 2.5 was followed with double incubation times at each step and overnight fixation. The

quantitative RT-PCR analysis was exactly the same as Section 2.7 with exception of homogenization with insulin syringe for 30-40 times instead of 12.

2.10. Three Dimensional (3D) Cell Culture via Whatman Paper

Whatman paper (GE Healthcare Life Sciences Ca#1114-240) were cut to fit 24-well plates. Then they were placed in wells and 1 ml 96% ethanol was added on top of papers. Papers were left for 2 hours and then ethanol was aspirated and papers were left to dry overnight. Then HaCaT cell lines (10^4 per well) were plated in each well. After papers absorbed cells, 2 ml DMEM was added in wells and cells were incubated for a week (37^oC, 5% CO_2). Then, immunostaining was performed as explained in Section 2.5 with Whatman paper.

To construct more complex 3D cell culture with Whatman paper; paper was prepared similarly. Instead of plating HaCaT cell lines directly, first NIH3T3 (10^4 per well) cells were planted on top of Whatman paper. 2 ml DMEM was added in wells. After couple days of incubation (37^oC, 5% CO_2), generated HaCaT cell lines (10^4 per well) were added on top of NIH3T3 cell. Then cells were again incubated for two of days. Finally air-liquid surface generated and cells left to differentiate for 21 days and DMEM was refreshed every 3 days.

CHAPTER 3

RESULTS AND DISCUSSIONS

3.1. Virus Titration

Efficiency of produced viruses was determined by virus titration. NIH3T3 cells were infected with each virus type (MSCV, Cx26WT and Cx26D50Y) and after selection, colonies were counted (Table 4). Titration results showed that there was a significant difference between generated vectors in terms of efficiency. MSCV vector seems to outperform other at two different titration assay. MSCV was three times more efficient than Cx26D50Y. Cx26WT was less efficient than MSCV but two times more efficient than Cx26D50Y. This result was expected because MSCV contains just empty vector without Cx26 gene so any secondary structure introduced by Cx26 gene that may affect packaging of the plasmid is not present [98]. On the other hand, the reason behind efficiency difference between Cx26WT and Cx26D50Y viral vectors was not clear but can be caused by again packaging difference between vectors.

Tablo 4. Colony Count of Titration Assay.

Vector Type	**Titration Assay 1 Colony Count**	**Titration Assay 2 Colony Count**
MSCV	93	128
Cx26WT	54	77
Cx26D50Y	21	38

3.2. Infection and Generation of Stable Cell Lines

Titration assay results were used to adjust the amount of viruses used for infection of HaCaT cells. Cells are needed to contain approximately similar amount of

introduced DNA for experiments. Otherwise, the reason behind observed differences between generated cell lines cannot be deduced. Reason can be either Cx26 type or the number of Cx26. Then, cells were infected and selected to generate stable cell lines. Different from transient transfection, generating stable cell lines provides several advantages such as; increased reproducibility, integration to host genome, long term protein expression and reduced effects of environmental factors on expression [99]. In the end, stable HaCaT cell lines were generated and confirmed by EGFP signal (Figure 6). Infection and generation of stable HaCaT lines were performed three times. Cells were observed under fluorescence microscope to monitor green signal each week. Gradual green signal loss was observed with each increased passage number for all cell line (data not shown). After third transfection, selection medium was used every other week and passage number was kept low in order to prevent such signal loss at our cell lines. These cell lines did not lose green signal even at passage number 17 (Figure 6).

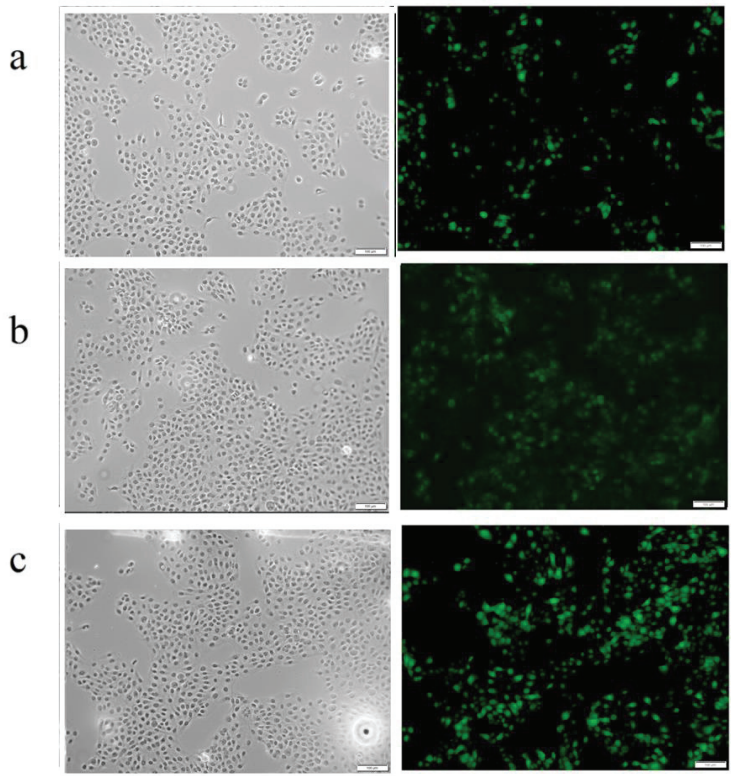

Figure 6. Microscope images of generated stable cell lines. Phase-contrast images and green signal (EGFP) images are presented side by side. Generated stable cell lines are MSCV (a), Cx26WT (b) and Cx26D50Y (c). Magnification is 10X and scale bar represents 100 μm.

3.3. Cx26 Expression at Generated Cell Lines

After generation of the cell lines, Cx26 expression was checked. Our aim is to utilize those cell lines to make a 3D KID syndrome model so our key factor was Cx26. In order to check distribution of the Cx26 and its amount of expression, immunostaining was performed (Figure 7). Immunostaining of Cx26 protein showed that Cx26WT and Cx26D50Y cell lines had Cx26 expression as expected (Figure 7 b and c) but MSCV (cell line with empty vector, used as negative control) also had Cx26 (Figure 7a).

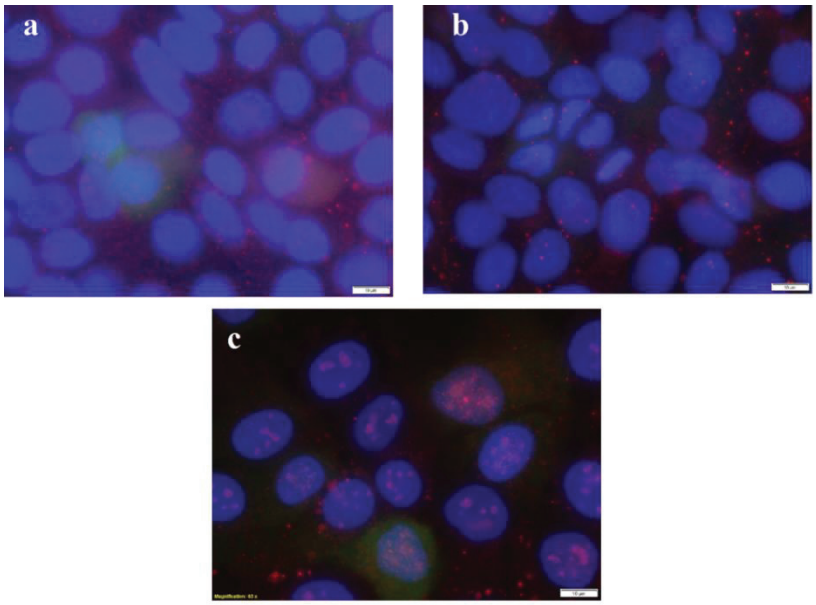

Figure 7. Determination of Cx26 localization and expression in stable HaCaT cell lines. Staining was performed with MSCV (a), Cx26WT (b) and Cx26D50Y (c). Blue color is DAPI, green is EGFP and red dots are Cx26. Magnification is 100X and scale bar represents 10 μm.

Before reaching any conclusion, untransfected HaCaT cells were used to double check as another negative control (Figure 8). Like empty vector transfected MSCV cells, untransfected HaCaT cells also had Cx26 protein. Cx26 is present at basal keratinocytes and its expression is seen in the palmoplantar epidermis [56]. Other studies also showed that HaCaT cells show basal keratinocyte features [100]. These studies support our findings which indicate HaCaT cells have Cx26. Even though pictures were taken at the same exposure time, it is hard to tell whether cell lines were

different from each other in terms of connexin protein amount. But in terms of localization, Cx26D50Y cells have clustered Cx26 signals near or on top of DAPI signal. Previously, it is reported that Cx26D50Y mutation causes retention of the Cx26 in the Golgi apparatus [87]. So seen localization difference of Cx26 signal can be result of retention of the mutant Cx26 in the Golgi apparatus.

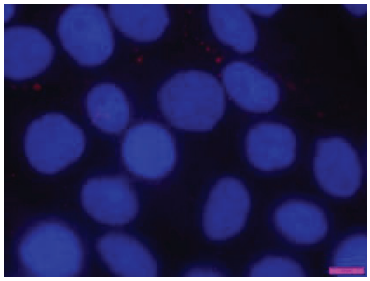

Figure 8. Determination of Cx26 localization and expression in untransfected HaCaT cells. Blue color is DAPI and red color represents Cx26. Magnification is 100X and scale bar represents 10 μm.

In order to detect differences at Cx26 protein levels in MSCV, WT and D50Y stable cell lines, Western blot analysis was used (Figure 9). According to this; WT and D50Y cell lines had 1.5 fold increase in Cx26 protein level compared to MSCV ($p<0.05$ and $n=6$). This means that mutant and wild type Cx26 infected cell lines produced wild type and mutant Cx26 protein.

Like protein levels, qRT-PCR results showed that WT and D50Y stable cell lines had more Cx26 mRNA in comparison to MSCV cell line (Figure 10). These results are consistent with our Western blot analysis and confirmed that wild type and mutant Cx26 gene was successfully integrated into HaCaT cell lines. Figure 10 also shows that there is a variation between cell lines. Although infection was performed according to titration result, Cx26WT mRNA level was higher than Cx26D50Y. This variation can be caused by variation at infection. Also, each passing passage number may cause this variation but cells were only used up to passage number 15 and selection performed with cell at every third passage. Another suspect is differences at mutations themselves meaning some kind of control mechanism cause Cx26D50Y mRNA degradation but further analysis and confirmation are needed.

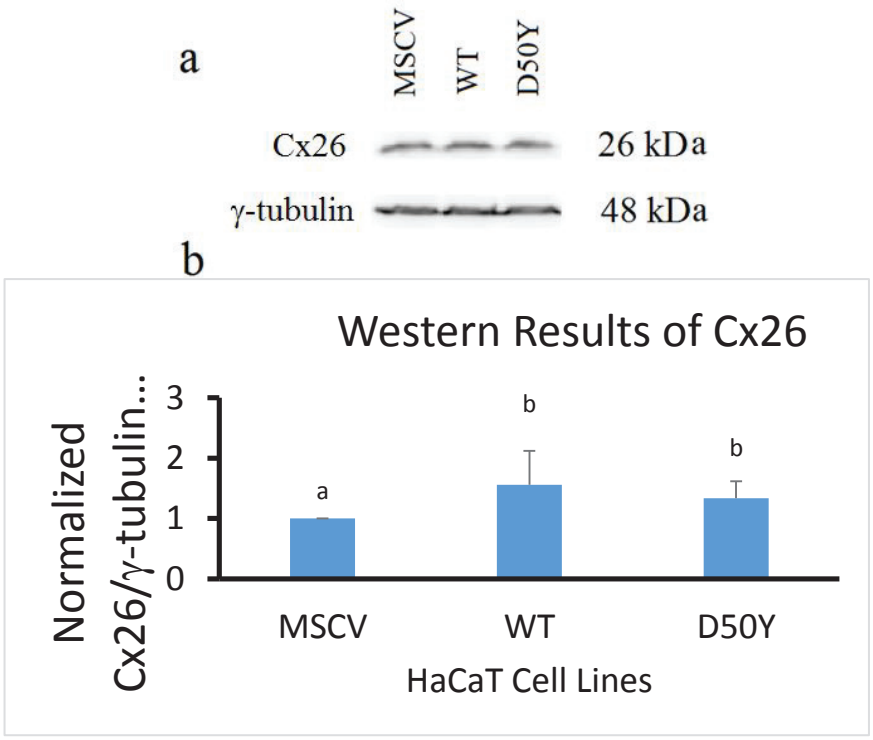

Figure 9. Comparison of Cx26 protein levels in stable HaCaT cell lines. (a) Representative Western blot gel image. Cx26 gives band at 26 kDa. As a loading control, γ-tubulin (48 kDa) was utilized. (b) Comparison of Cx26 band intensity ratios relative to γ-tubulin. Different letter indicates significant difference at $p<0.05$ as determined by Tukey's HSD (n=6).

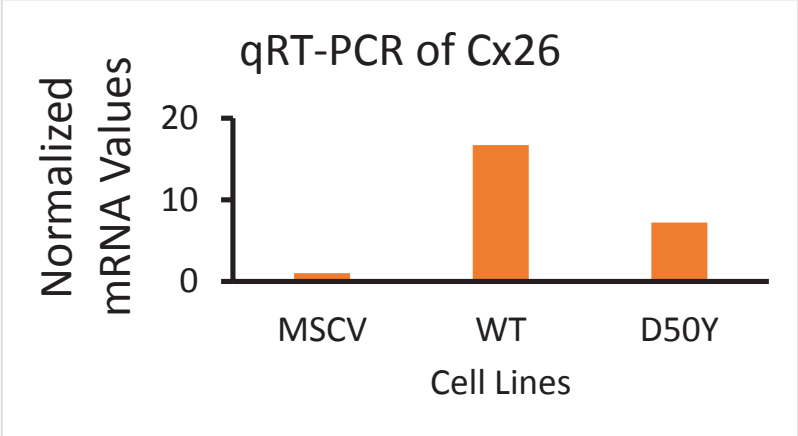

Figure 10. Cx26 mRNA expression levels of HaCaT cells lines. For housekeeping control GAPDH gene was utilized. Normalization was done according to MSCV expression levels.

3.4. Cx43 Expression changes in Generated Cell Lines

As mentioned in the introduction, connexin molecules can form heteromeric connexons [14] but not all connexins are compatible to form heteromeric channels, for example, Cx26 and Cx43 do not form heteromeric channels [101]. It is shown that syndromic Cx26 mutations at amino terminus (including KID mutants) had altered oligomerization compatibility, resulting in the formation of heteromeric Cx43/Cx26 connexons. These heteromeres increase cell membrane permeability to ATP and Ca^{2+} when compared to homomeric wild type Cx26 in HeLa cells [89]. So visualization of connexin 43 was performed in order to see whether our cell lines shows difference at Cx43 expression due to Cx26 mutation. As seen in figure 11, all stable cell lines showed Cx43 expression.

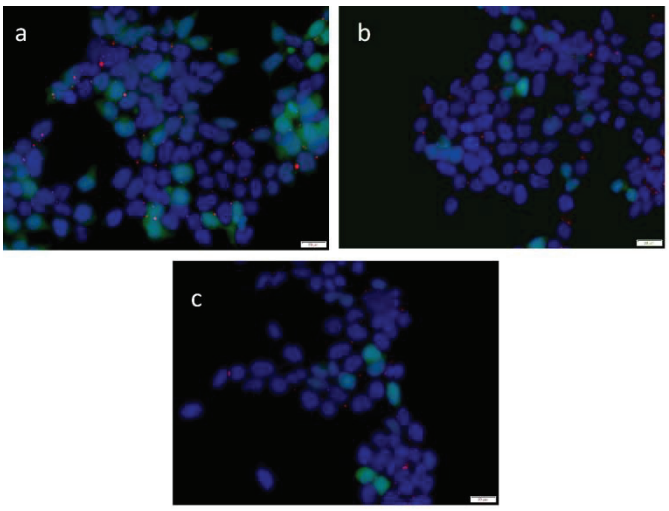

Figure 11. Determination of Cx43 localization and expression in stable HaCaT cell lines. Staining was performed with MSCV (a), Cx26WT (b), Cx26D50Y (c). Blue color is DAPI staining, green is EGFP and red is Cx43. Magnification is 40X and scale bar represents 20 μm.

Similarly, in order to detect differences at protein levels of Cx43, Western blot was used (Figure 12). According to our results; WT and D50Y cell lines had 1.5 fold increase in Cx43 protein level when compared to MSCV ($p<0.05$ and $n=4$). This indicates that overexpression of Cx26 either wild type or mutant caused an increase in

Cx43 protein levels. Further, mRNA levels were also checked by qRT-PCR. All stable cell lines were used in qRT-PCR (Figure 13).

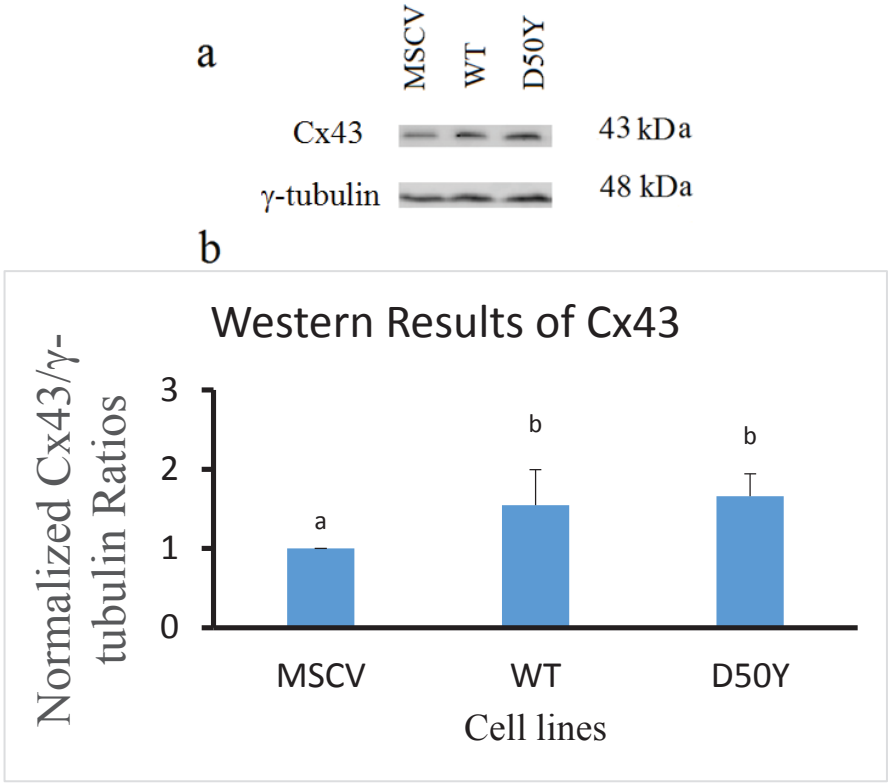

Figure 12. Comparison of Cx43 protein levels in stable HaCaT cell lines. (a) Nitrocellulose images of the analysis. Cx43 gives band at 43 kDa and loading control γ-tubulin gives band at 48 kDa. (b) Graphical representation of intensity ratios of protein bands. Different letter indicates significant difference at $p<0.05$ as determined by Tukey's HSD (n=4).

According to our findings, mRNA levels of the cell lines were similar to each other so infection with Cx26 did not affect cytoplasmic mRNA levels of Cx43. In short, increased Cx26 expression seems to increase Cx43 protein levels but it fails to change Cx43 mRNA levels. Cx43 has short half-life of around 1.3 hours [102]. Thus, Cx26 expression may increase the half-life of Cx43 protein so more protein might be observed in Cx26 overexpression.

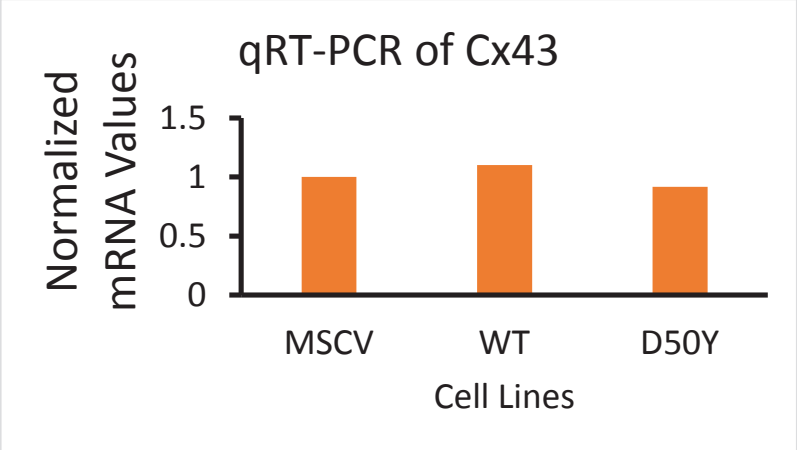

Figure 13. Cx43 mRNA expression levels of HaCaT cells lines. For housekeeping control GAPDH gene was utilized. Normalization was done according to MSCV expression levels.

3.5. Immunostaining of Epidermal Differentiation Markers

In order to construct three dimensional organotypic culture, first generation of stable cell lines and confirmation of the success of infection by immunostaining, Western blot and qRT-PCR of the Cx26 was performed. As mentioned before, keratinocytes in the epidermis form protective barrier by their differentiation process [97]. During construction of organotypic culture, our generated cell lines need to form skin layers by undergoing differentiation process. Each layer shows different expression level of some proteins namely filaggrin, loricrin, involucrin and cytokeratins [96]. Cytokeratin 14, cytokeratin 10 and involucrin were used as molecular markers of epidermis differentiation. Cytokeratin 14 is mainly expressed in basal spinous layer, involucrin mostly present in corneum layer and cytokeratin 10 is expressed between those layers [96, 103, 104]. So, first differentiation state of generated cell lines was checked via immunostaining of Cytokeratin 14, cytokeratin 10 and involucrin in 2D cultured cells. As seen in figure 14, all samples showed cytokeratin 14 expression. These results are compatible with the literature. As stated, HaCaT cells show basal spinous layer keratinocyte characteristics [100] and cytokeratin 14 is a basal layer marker [104].

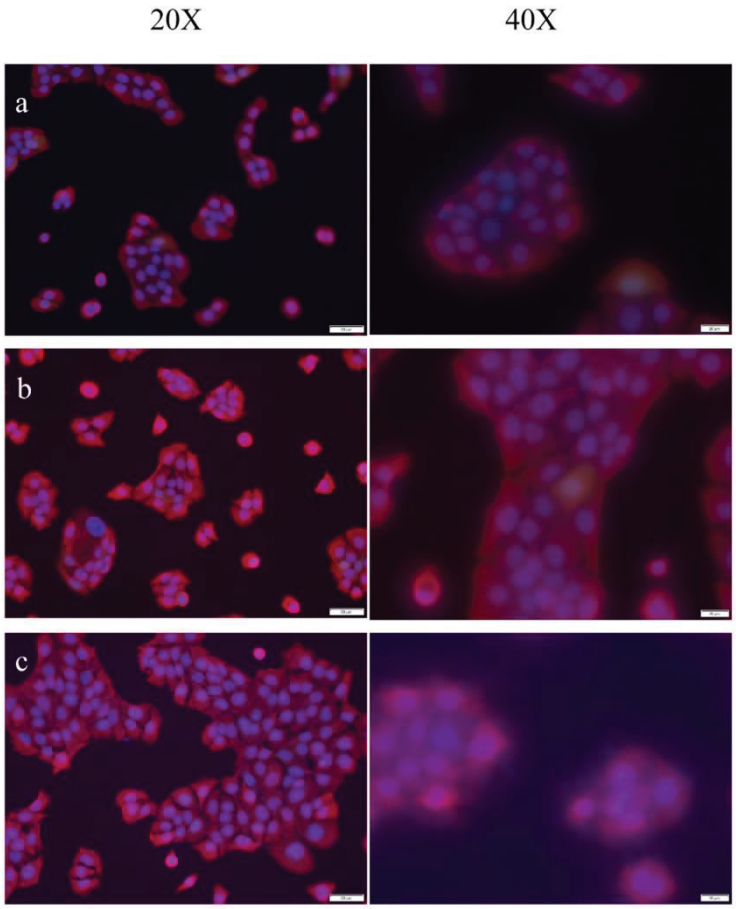

Figure 14. Demonstration of differentiation marker Cytokeratin 14 in stable HaCaT cell lines. Staining was performed with MSCV (a), Cx26WT (b), and Cx26D50Y (c). Blue color is DAPI staining, green is EGFP and red is Cytokeratin 14. Magnifications are 20X and 40X. Scale bars represent 50 μm and 20 μm respectively.

Cytokeratin 10 on the other hand, was detected in couple of cells in each staining (Figure 15). Number of Cytokeratin 10 expressing cells seemed to have correlation between confluency of the cells and similar results have been published before stating cytokeratin 1 and 10 expression increases with HaCaT cell density of [105]. Further, it is reported that increased confluency of the cells induces HaCaT differentiation [106]. Thus, these Cytokeratin 10 expressing cells can be at early stages of differentiation.

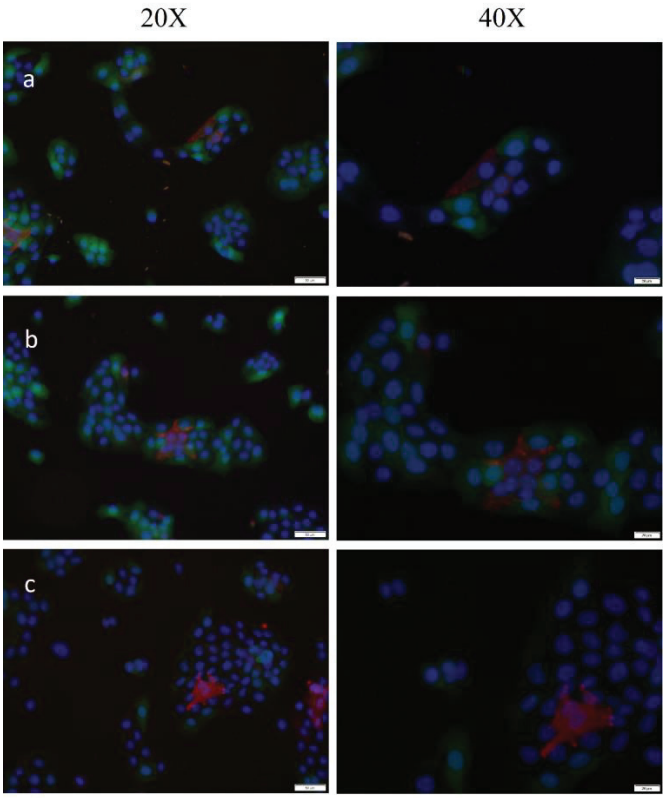

Figure 15. Demonstration of differentiation marker Cytokeratin 10 in stable HaCaT cell lines. Staining was performed with MSCV (a), Cx26WT (b), and Cx26D50Y (c). Blue color is DAPI staining, green is EGFP and red is Cytokeratin 10. Magnifications are 20X and 40X. Scale bars represent 50 μm and 20 μm respectively.

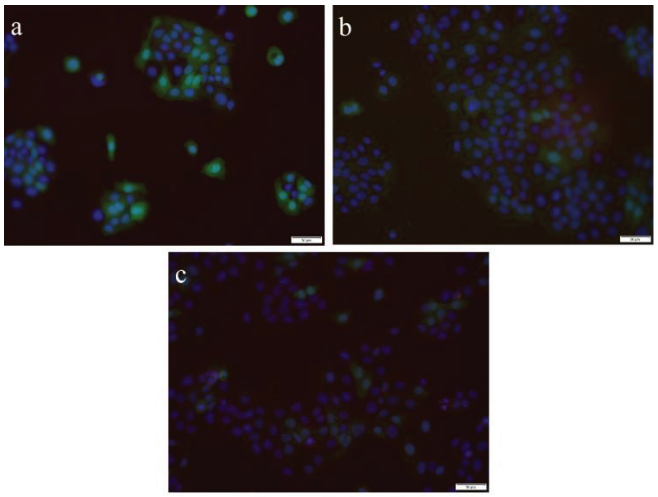

Figure 16. Demonstration of differentiation marker involucrin in stable HaCaT cell lines. Staining was performed with MSCV (a), Cx26WT (b), and Cx26D50Y (c). Blue color is DAPI staining, green is EGFP and red is involucrin. Magnification is 20X and scale bar represents 50 μm.

Finally, involucrin staining was performed and generated cell lines did not have any involucrin. So no cell was at terminal stage of differentiation. This is expected because HaCaT cells do not normally differentiate without factors such as increased Ca^{2+} concentration or increased cell density [107].

All differentiation markers also used with untransfected HaCaT cells to check whether infection changes expression of these differentiation markers. As seen in figure 16, untransfected HaCaT cells had similar expression of cytokeratin 14 (Figure 17a), cytokeratin 10 (Figure 17b) and involucrin (Figure 17c). Overall these findings show that, generated WT and mutant Cx26 expressing cells works as intended and can be used to generate 3D culture.

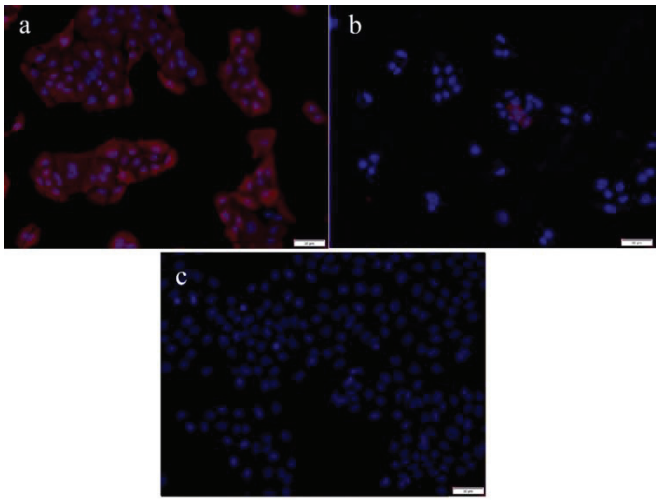

Figure 17. Demonstration of differentiation markers at untransfected HaCaT cells. Cytokeratin 14 (a), Cytokeratin 10 (b) and involucrin (c) markers were used. Staining was performed with untransfected HaCaT cells. Blue color is DAPI staining. Cytokeratin 14, cytokeratin 10 and involucrin are red signal. Magnification is 20X and scale bar represents 50 μm.

3.6. Cell Viability Assay

Assessing differences between mutant Cx26 containing cell lines and wild type Cx26 containing cell lines is one of the focuses of this study. Several studies had linked Cx26 mutations with increased cell death [85, 86, 108]. So, MTT cell viability assay was performed to see any viability difference between stable cell lines (Figure 18).

Assay results showed that this is not the case for our cell lines. They did not have any viability difference between them.

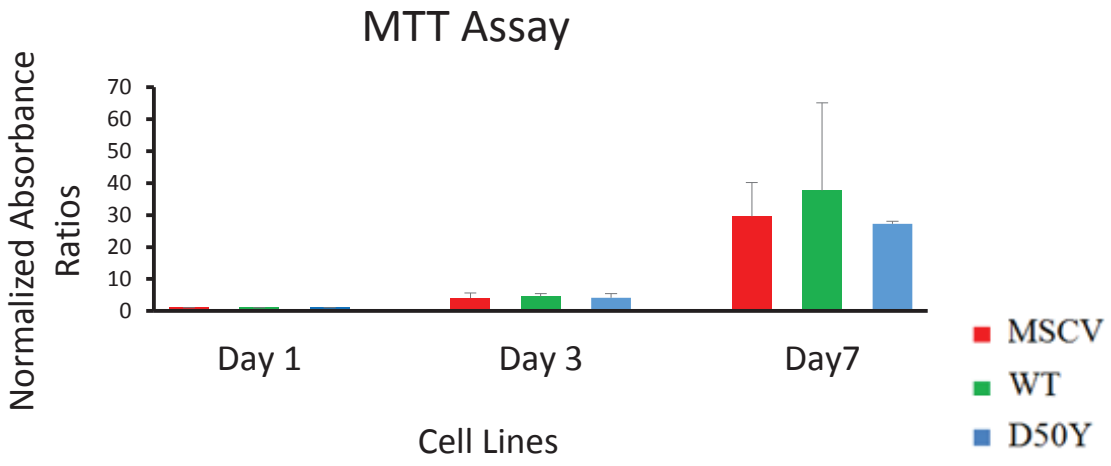

Figure 18. Cell viability results of generated cell lines via MTT assay. MSCV, Cx26WT, and Cx26D50Y cell lines were used. Measurements performed at day 1, 3 and 7. Results of each cell type normalized with its corresponding day 1 result.

3.7. Organotypic Culture of HaCaT Cell Lines with Transwell Inserts

Several 3D culture methods have been generated for different tissues and used for various purposes from treatment to drug tests to pure science applications [109]. Skin is just one of the tissues constructed via 3D culture methods but skin constructing is arguably one of the more established area in this context. In order to perform a 3D skin construction, several different methods are available [110]. Between those options, commercially available inserts is a widely accepted way of skin construction [110, 111]. In order to mimic condition in the skin, first a fibroblast collagen mixture was placed in the insert. This layer corresponds to connective tissue under the epidermis. Then HaCaT cells placed on top of fibroblast collagen mixture to act as basal layer of the epidermis. These cells were allowed to divide and with the help of air-liquid surface formed by the insert to differentiate. In the end, 3D constructs were generated. As seen in both figures 19 and 20, DAPI and EGFP were observed showing cells in the inserts. This was promising and means constructions had intended cell lines. In figure 19, Cx26 staining

results did not show any signal so optimization process continues for this staining. Cytokeratin 14 staining images of the skin constructs (Figure 20) showed that MSCV and WT cells covered the surface of collagen but D50Y formed clusters. This can be result of an experimental error or can be caused by D50Y mutation. So this staining will be repeated for D50Y cell line to eliminate errors. As seen in figure 20, all cell lines regardless of the type produce cytokeratin 14 so basal layer present at our constructs. This result made us one step closer to the goal of producing 3D model for KID syndrome. But confirmation of other layers with cytokeratin 10 and involucrin is needed and is in the process.

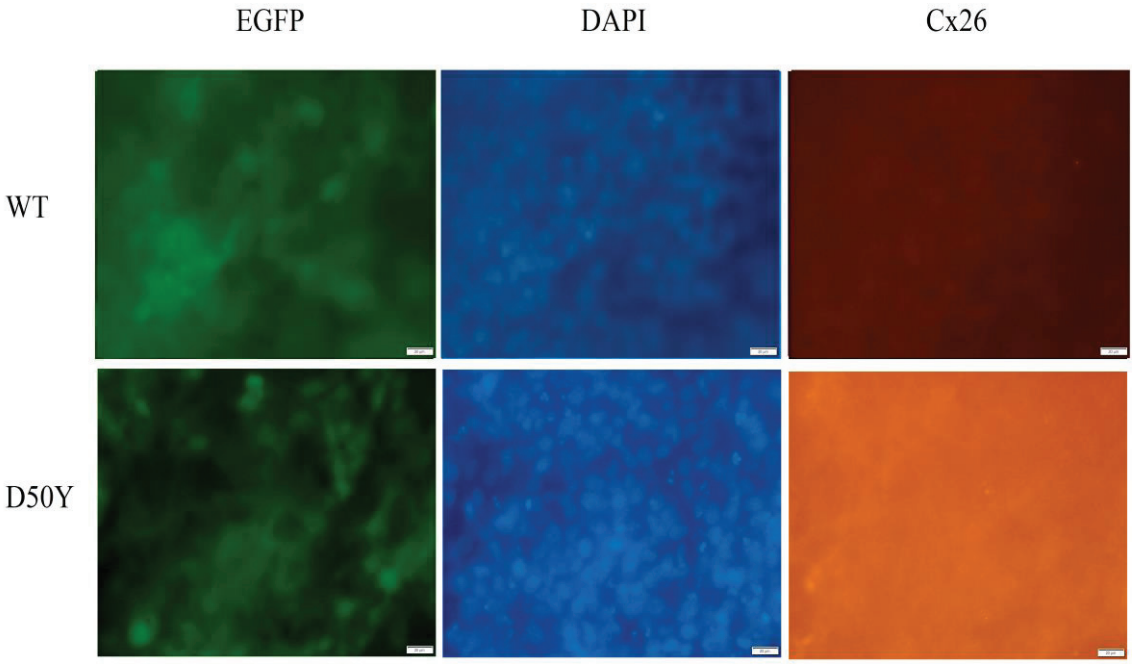

Figure 19. Detection of Cx26 localization and expression in skin constructs. Staining was performed with Cx26WT and Cx26D50Y. Blue color is DAPI, green is EGFP and red is Cx26. Magnifications are 20X. Scale bar represents 50 µm.

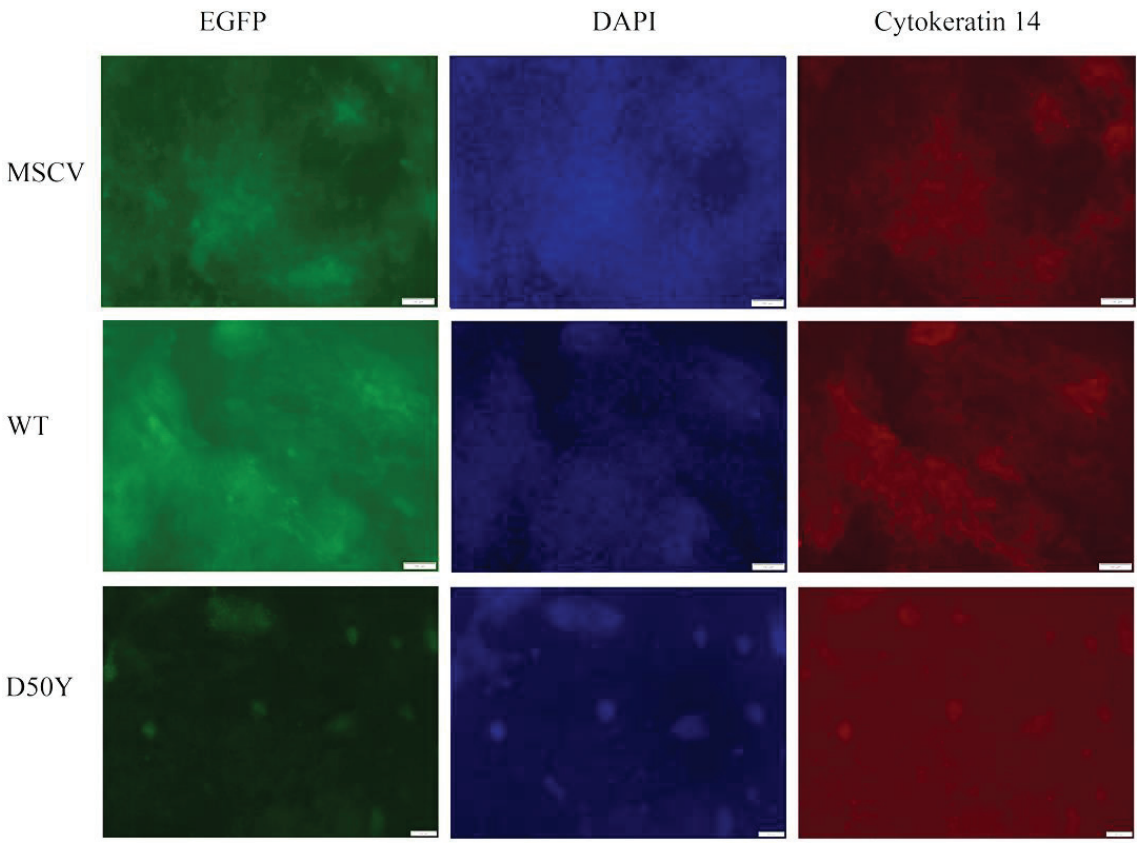

Figure 20. Detection of cytokeratin 14 localization and expression in skin constructs. Staining was performed with MSCV and Cx26WT. Blue color is DAPI, green is EGFP and red is Cx26. Magnification is 10X and Scale bar represents 100 μm.

3.8. Three Dimensional (3D) Cell Culture via Whatman Paper

Recently, different studies have taken advantage of properties of paper and used it as cell culture substrate. Biocompatibility of paper and its cost makes it a suitable candidate for constructing 3D culture platform and ability to stacking into a 3D structure provides means to control distribution of cells and the extracellular matrix [112]. Whatman paper was utilized to construct simple artificial 3D cell culture model as an alternative to transwell inserts. In order to check whether HaCaT cells can survive and proliferate in Whatman paper, culture model was constructed. After construction of the culture model, cells were investigated via immunostaining of DAPI and phalloidin. As seen in figure 21, generated cell lines were managed to attach cellulose fibers and formed cell clusters. When magnification increased to get a closer look, DAPI images

taken at two different z-stack at the same place showed that cells formed 3D structures with help of cellulose fibers (Figure 22).

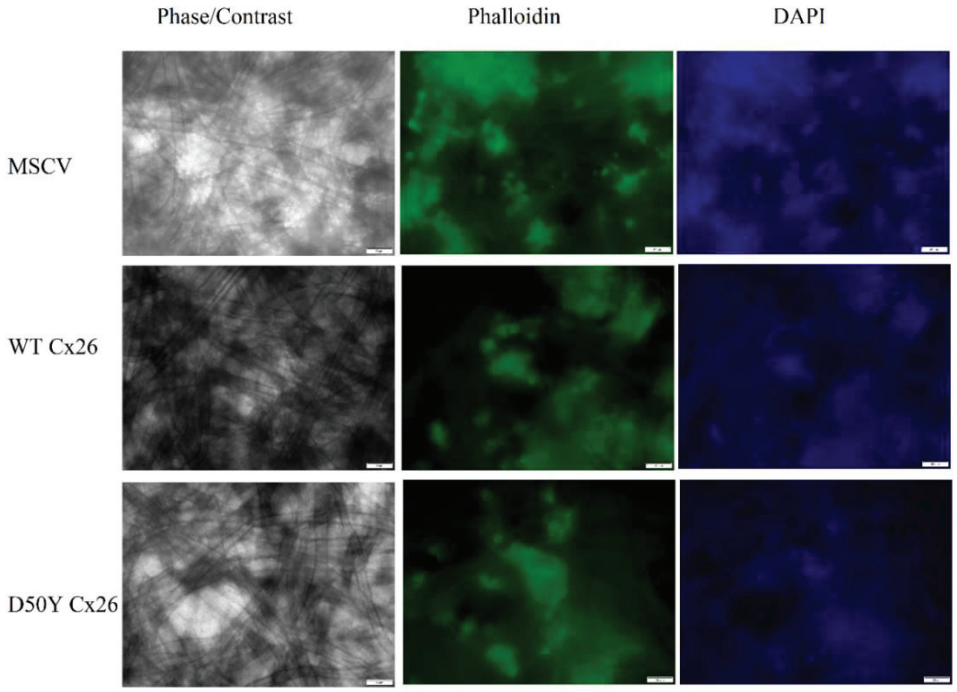

Figure 21. Visualization of HaCaT cell lines via phalloidin and DAPI staining. Staining was performed with MSCV, Cx26WT and Cx26D50Y. Phase/Contrast, DAPI and phalloidin staining images of the same area were taken for each cell line. Magnification is 20X and scale bar represents 50 µm.

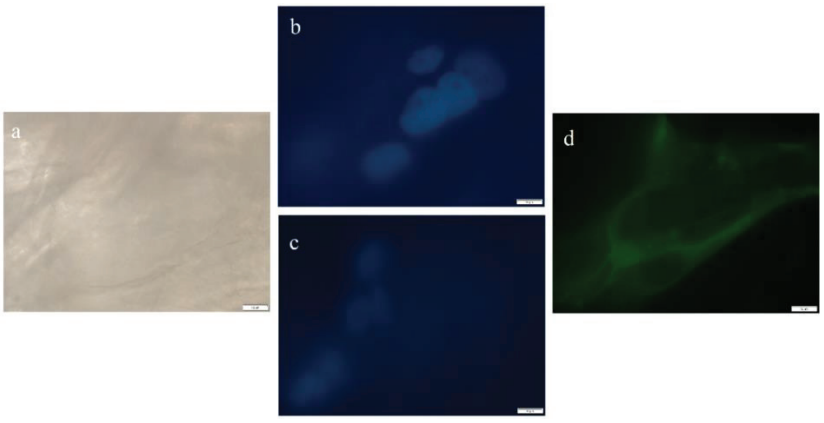

Figure 22. High magnification of phalloidin immunostaining. Phase/Contrast (a), different focus depth of DAPI (b and c) and phalloidin staining (d). Magnification is 100X and scale bar represents 00 µm.

Then more complex 3D models based on Whatman paper designed to mimic KID syndrome and model investigated via immunostaining of epidermal differentiation markers. As seen in the Figure 23, 3D constructs regardless to cell line, gave cytokeratin 14 signal, the basal layer marker. These results were similar to 3D transwell constructs results and indicated that basal layer was present in 3D cell culture. On the other hand, Whatman paper constructs also showed cytokeratin 10 signal (Figure 24). When compared to 2D staining results, cytokeratin 10 staining suggested that cells started to differentiate to form other skin layers.

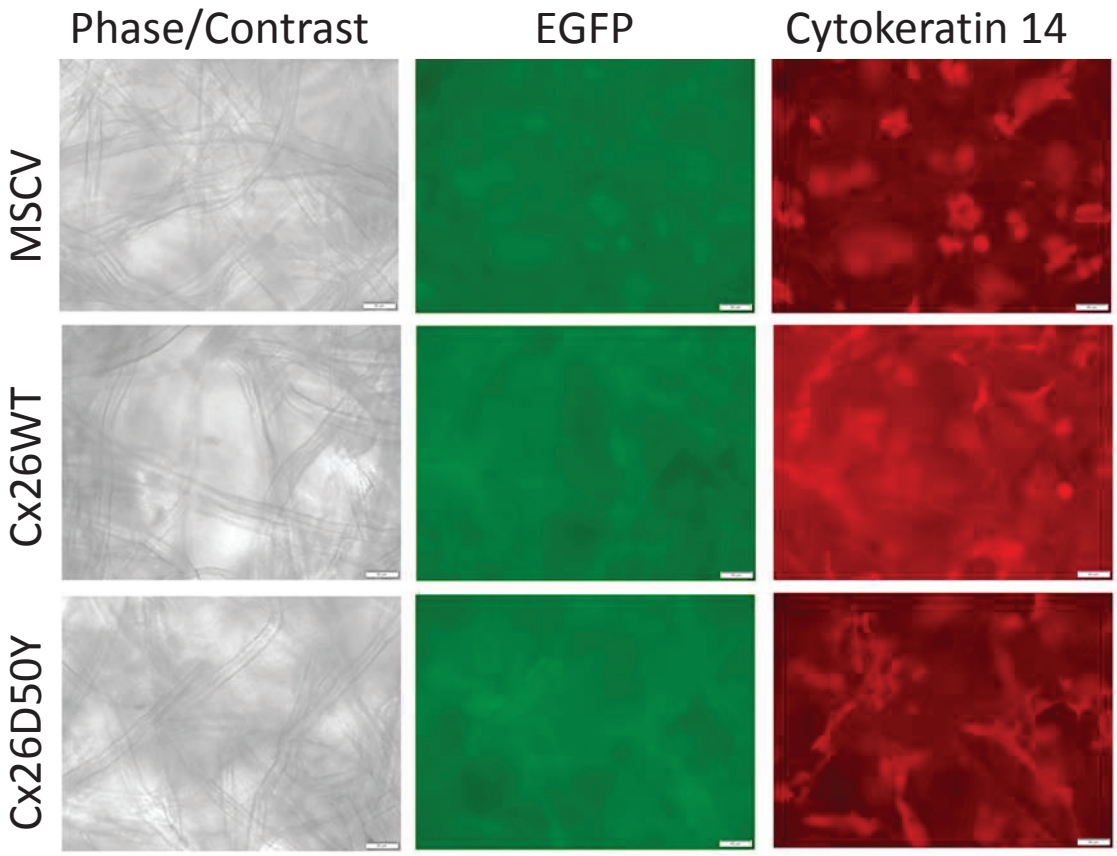

Figure 23. Differentiation evaluation of HaCaT cell lines via cytokeratin 14 staining. Staining was performed with MSCV, Cx26WT and Cx26D50Y. Phase/Contrast, EGFP and cytokeratin 14 images of the same area were taken for each cell line. Magnification is 20X and scale bar represents 50 µm.

Finally involucrin was checked and as seen in figure 25, cell lines did not have involucrin signal. This indicates that cells did not go to terminal stage of differentiation and did not form corneum layer. So optimization is still needed to generate construct with all epidermal layers.

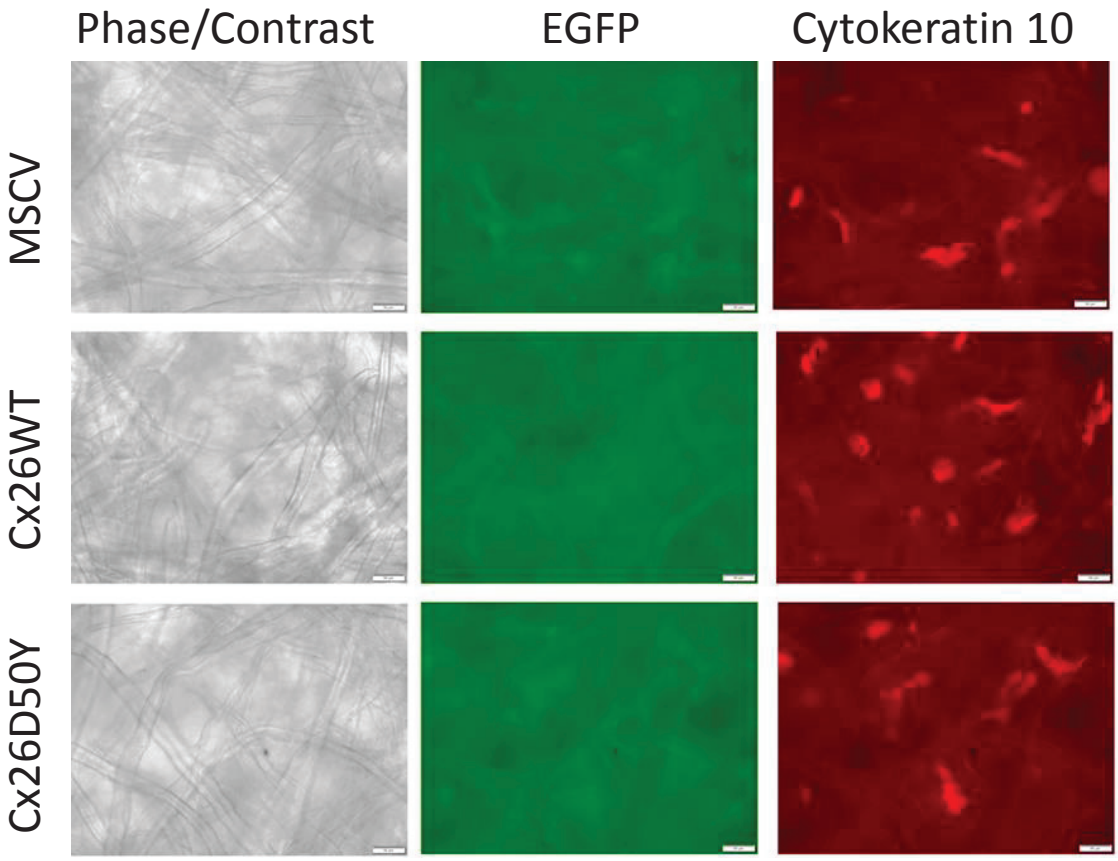

Figure 24. Differentiation evaluation of HaCaT cell lines via cytokeratin 10 staining. Staining was performed with MSCV, Cx26WT and Cx26D50Y. Phase/Contrast, EGFP and cytokeratin 10 images of the same area were taken for each cell line. Magnification is 20X and scale bar represents 50 µm.

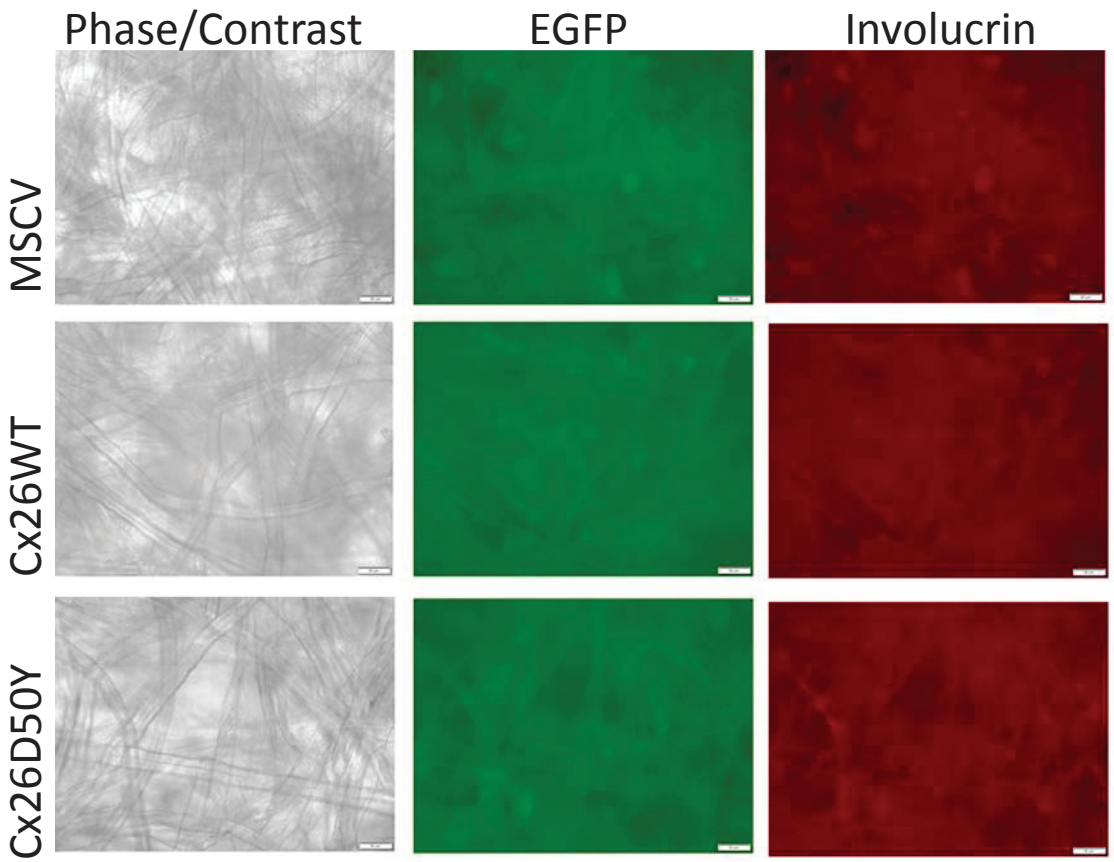

Figure 25. Differentiation evaluation of HaCaT cell lines via involucrin staining. Staining was performed with MSCV, Cx26WT and Cx26D50Y. Phase/Contrast, EGFP and involucrin images of the same area were taken for each cell line. Magnification is 20X and scale bar represents 50 μm.

CHAPTER 4

CONCLUSION

KID syndrome is a quite complex syndrome with complicated symptoms that affect different organs, difference in symptoms from patient to patient and heterogeneity at the genetic level. Because the syndrome is rare and usually accompanied by a superinfection, getting biopsy samples are not easy. On the other hand, 2D culture methods fell short to provide complex and close to real conditions to investigate various abnormalities of KID syndrome on skin that change from patient to patient. Here we tackle this problem via construction of organotypic 3D skin model for the KID syndrome.

As a first step, HaCaT cell lines that contain mutant and wild type Cx26 were generated and confirmed with combined results of Western blot, immunostaining and qRT-PCR. These cell lines provided opportunities to see effects of Cx26 in 2D culture. Our analysis on Cx43 showed that Cx26 up-regulation caused an increase at Cx43 protein levels. These results seem as one of the missing puzzle piece about KID syndrome. As stated before Cx26 and Cx43 are not compatible connexins to form heterotypic connexons but amino terminus mutation of Cx26 (which includes some KID syndrome mutations), can cause formation of aberrant connexon composed of Cx26 and Cx43 [87]. It is also speculated that this aberrant heterotypic connexon formation can be responsible for various skin complications seen at KID syndrome. So our findings add another layer to complexity by stating Cx26 up-regulation increased Cx43 protein level. Because mRNA level difference was not detected, we can say that Cx26 up-regulation somehow increased protein stability of Cx43 but it is not known whether this result caused by Cx26 mRNA or Cx26 protein or even combination of both.

Several works showed that Cx26 mutations decrease cell viability [85, 86, 103]. But here we did not see detectable difference in cell viability in HaCaT cells caused by wild type or D50Y mutant Cx26 protein level. Behind this can be the nature of HaCaT cells; as there are other connexins in these cells that can compensate for the effect of mutant Cx26D50Y and our results also suggested that untransfected HaCaT cells had

WT Cx26 expression. In terms of differentiation, immunostaining results of cytokeratin 14, 10 and involucrin confirmed basal characteristics of HaCaT cells.

Our main goal was constructing 3D skin model for the KID syndrome. With the help of transwell inserts, construction of a skin model that have fibroblast-collagen layer and basal epidermis layer composed of either wild type or D50Y mutant Cx26 expressing HaCaT cells had been accomplished. It is not clear whether basal layer cells formed other epidermis layers or not. So next step ahead is to show other epidermis layers if differentiation occurred or if not, assist differentiation process by known factors such as increasing Ca^{2+} concentration or HaCaT cell density.

In recent years, different studies have taken advantage of biocompatibility and cost of paper to construct 3D culture. So as an alternative to skin constructed via transwell inserts, Whatman paper was used. Our simple culture results showed that generated cell lines attached to cellulose fibers, formed cell clusters and 3D structures with the help of cellulose fibers. When more complex 3D model based on Whatman paper was designed; construct gave cytokeratin 14 signal indicating presence of basal layer and cytokeratin 10 signal suggesting that cell lines started to differentiate to form other skin layers. This means Whatman paper can be utilized for constructing more complex 3D cultures so our next step is to generate skin with help of Whatman paper that is composed of all epidermal layers to investigate the molecular mechanisms leading to KID syndrome.

After confirming construction of 3D skin model for the KID syndrome; processes that lead to KID syndrome, effects of aberrant connexons and complexity of connexin-connexin interactions can be investigated by comparison of organotypic KID syndrome model to its wild type counterpart. Successful construction of organotypic skin model of KID syndrome will also provide easily accessible, fungal or bacterial infection free samples. These skin constructs can help drug testing and can be a guide to other KID syndrome skin constructs containing different mutations.

REFERENCES

1. Kumar, N.M. and N.B. Gilula, *The gap junction communication channel.* Cell, 1996. 84(3): p. 381-8.

2. Laird, D.W., *The gap junction proteome and its relationship to disease.* Trends Cell Biol, 2010. 20(2): p. 92-101.

3. Evans, W.H. and P.E. Martin, *Gap junctions: structure and function (Review).* Mol Membr Biol, 2002. 19(2): p. 121-36.

4. Kleopa, K.A. and I. Sargiannidou, *Connexins, gap junctions and peripheral neuropathy.* Neurosci Lett, 2015. 596: p. 27-32.

5. Harris, A.L., *Emerging issues of connexin channels: biophysics fills the gap.* Q Rev Biophys, 2001. 34(3): p. 325-472.

6. Valiunas, V., et al., *Connexin-specific cell-to-cell transfer of short interfering RNA by gap junctions.* J Physiol, 2005. 568(Pt 2): p. 459-68.

7. Phelan, P. and T.A. Starich, *Innexins get into the gap.* BioEssays, 2001. 23(5): p. 388-396.

8. Severs, N.J., et al., *Remodelling of gap junctions and connexin expression in diseased myocardium.* Cardiovasc Res, 2008. 80(1): p. 9-19.

9. Gerhart, S.V., R. Jefferis, and M.K. Iovine, *Cx40.8, a Cx43-like protein, forms gap junction channels inefficiently and may require Cx43 for its association at the plasma membrane.* FEBS Lett, 2009. 583(21): p. 3419-24.

10. El-Sabban, M.E., L.F. Abi-Mosleh, and R.S. Talhouk, *Developmental regulation of gap junctions and their role in mammary epithelial cell differentiation.* J Mammary Gland Biol Neoplasia, 2003. 8(4): p. 463-73.

11. Sohl, G. and K. Willecke, *Gap junctions and the connexin protein family.* Cardiovascular Research, 2004. 62(2): p. 228-232.

12. Forge, A., et al., *Gap junctions in the inner ear: comparison of distribution patterns in different vertebrates and assessement of connexin composition in mammals.* J Comp Neurol, 2003. 467(2): p. 207-31.

13. Beltramello, M., et al., *Impaired permeability to Ins(1,4,5)P3 in a mutant connexin underlies recessive hereditary deafness.* Nat Cell Biol, 2005. 7(1): p. 63-9.

14. Sun, J., et al., *Cochlear gap junctions coassembled from Cx26 and 30 show faster intercellular Ca2+ signaling than homomeric counterparts.* Am J Physiol Cell Physiol, 2005. 288(3): p. C613-23.

15. Mathias, R.T., T.W. White, and X. Gong, *Lens gap junctions in growth, differentiation, and homeostasis.* Physiol Rev, 2010. 90(1): p. 179-206.

16. Sohl, G. and K. Willecke, *Gap junctions and the connexin protein family.* Cardiovasc Res, 2004. 62(2): p. 228-32.

17. Gray, K.A., et al., *Genenames.org: the HGNC resources in 2013.* Nucleic Acids Res, 2013. 41(Database issue): p. D545-52.

18. Saez, J.C., et al., *Gap-Junctions - Multiplicity of Controls in Differentiated and Undifferentiated Cells and Possible Functional Implications.* Advances in Second Messenger and Phosphoprotein Research, 1993. 27: p. 163-198.

19. Söhl, G. and K. Willecke, *An Update on Connexin Genes and their Nomenclature in Mouse and Man.* Cell Communication & Adhesion, 2003. 10(4-6): p. 173-180.

20. Oh, S., V.K. Verselis, and T.A. Bargiello, *Charges dispersed over the permeation pathway determine the charge selectivity and conductance of a Cx32*

chimeric hemichannel. Journal of Physiology-London, 2008. 586(10): p. 2445-2461.

21. Hirst-Jensen, B.J., et al., *Characterization of the pH-dependent interaction between the gap junction protein connexin43 carboxyl terminus and cytoplasmic loop domains.* Journal of Biological Chemistry, 2007. 282(8): p. 5801-5813.

22. Maeda, S., et al., *Structure of the connexin 26 gap junction channel at 3.5[thinsp]A resolution.* Nature, 2009. 458(7238): p. 597-602.

23. Bao, X.Y., et al., *Functional expression in Xenopus Oocytes of gap-junctional hemichannels formed by a cysteine-less connexin 43.* Journal of Biological Chemistry, 2004. 279(11): p. 9689-9692.

24. Bergoffen, J., et al., *Connexin mutations in X-linked Charcot-Marie-Tooth disease.* Science, 1993. 262(5142): p. 2039-42.

25. Liu, X.Z., et al., *Mutations in the myosin VIIA gene cause non-syndromic recessive deafness.* Nat Genet, 1997. 16(2): p. 188-90.

26. Paznekas, W.A., et al., *Connexin 43 (GJA1) mutations cause the pleiotropic phenotype of oculodentodigital dysplasia.* Am J Hum Genet, 2003. 72(2): p. 408-18.

27. Laird, Dale W., *Life cycle of connexins in health and disease.* Biochemical Journal, 2006. 394(3): p. 527-543.

28. Kikuchi, T., et al., *Gap junctions in the rat cochlea: immunohistochemical and ultrastructural analysis.* Anat Embryol (Berl), 1995. 191(2): p. 101-18.

29. Chan, D.K. and K.W. Chang, *GJB2-associated hearing loss: systematic review of worldwide prevalence, genotype, and auditory phenotype.* Laryngoscope, 2014. 124(2): p. E34-53.

30. Di, W.L., et al., *Multiple epidermal connexins are expressed in different keratinocyte subpopulations including connexin 31.* J Invest Dermatol, 2001. 117(4): p. 958-64.

31. Martin, P.E., et al., *Connexins: sensors of epidermal integrity that are therapeutic targets.* FEBS Lett, 2014. 588(8): p. 1304-14.

32. Sbidian, E., et al., *Germline mosaicism in keratitis-ichthyosis-deafness syndrome: pre-natal diagnosis in a familial lethal form.* Clin Genet, 2010. 77(6): p. 587-92.

33. Menichella, D.M., et al., *Connexins are critical for normal myelination in the CNS.* J Neurosci, 2003. 23(13): p. 5963-73.

34. Shiels, A., T.M. Bennett, and J.F. Hejtmancik, *Cat-Map: putting cataract on the map.* Mol Vis, 2010. 16: p. 2007-15.

35. Kaba, R.A., et al., *Comparison of connexin 43, 40 and 45 expression patterns in the developing human and mouse hearts.* Cell Commun Adhes, 2001. 8(4-6): p. 339-43.

36. Van Norstrand, D.W., et al., *Connexin43 mutation causes heterogeneous gap junction loss and sudden infant death.* Circulation, 2012. 125(3): p. 474-81.

37. Kelly, J.J., J. Simek, and D.W. Laird, *Mechanisms linking connexin mutations to human diseases.* Cell Tissue Res, 2015. 360(3): p. 701-21.

38. Morell , R.J., et al., *Mutations in the Connexin 26 Gene (GJB2) among Ashkenazi Jews with Nonsyndromic Recessive Deafness.* New England Journal of Medicine, 1998. 339(21): p. 1500-1505.

39. Arora, A., et al., *A novel GJA8 mutation is associated with autosomal dominant lamellar pulverulent cataract: further evidence for gap junction dysfunction in human cataract.* J Med Genet, 2006. 43(1): p. e2.

40. Minogue, P.J., et al., *An aberrant sequence in a connexin46 mutant underlies congenital cataracts.* J Biol Chem, 2005. 280(49): p. 40788-95.

41. Das, S., et al., *ERp29 restricts Connexin43 oligomerization in the endoplasmic reticulum.* Mol Biol Cell, 2009. 20(10): p. 2593-604.

42. Laird, D.W., *Syndromic and non-syndromic disease-linked Cx43 mutations.* FEBS Lett, 2014. 588(8): p. 1339-48.

43. Gong, X.Q., et al., *A mechanism of gap junction docking revealed by functional rescue of a human-disease-linked connexin mutant.* J Cell Sci, 2013. 126(Pt 14): p. 3113-20.

44. Nakagawa, S., et al., *Asparagine 175 of connexin32 is a critical residue for docking and forming functional heterotypic gap junction channels with connexin26.* J Biol Chem, 2011. 286(22): p. 19672-81.

45. Beyer, E.C., L. Ebihara, and V.M. Berthoud, *Connexin Mutants and Cataracts.* Front Pharmacol, 2013. 4.

46. Tong, J.J., et al., *Properties of two cataract-associated mutations located in the NH2 terminus of connexin 46.* Am J Physiol Cell Physiol, 2013. 304(9): p. C823-32.

47. Saez, J.C., et al., *Cell membrane permeabilization via connexin hemichannels in living and dying cells.* Exp Cell Res, 2010. 316(15): p. 2377-89.

48. Sanchez, H.A., et al., *Differentially altered Ca2+ regulation and Ca2+ permeability in Cx26 hemichannels formed by the A40V and G45E mutations that cause keratitis ichthyosis deafness syndrome.* J Gen Physiol, 2010. 136(1): p. 47-62.

49. Churko, J.M., et al., *The potency of the fs260 connexin43 mutant to impair keratinocyte differentiation is distinct from other disease-linked connexin43 mutants.* Biochem J, 2010. 429(3): p. 473-83.

50. Dobrowolski, R., A. Sommershof, and K. Willecke, *Some oculodentodigital dysplasia-associated Cx43 mutations cause increased hemichannel activity in addition to deficient gap junction channels.* J Membr Biol, 2007. 219(1-3): p. 9-17.

51. Gemel, J., et al., *Degradation of a connexin40 mutant linked to atrial fibrillation is accelerated.* J Mol Cell Cardiol, 2014. 74: p. 330-9.

52. Diestel, S., et al., *Expression of a connexin31 mutation causing erythrokeratodermia variabilis is lethal for HeLa cells.* Biochem Biophys Res Commun, 2002. 296(3): p. 721-8.

53. Di, W.L., et al., *Defective trafficking and cell death is characteristic of skin disease-associated connexin 31 mutations.* Hum Mol Genet, 2002. 11(17): p. 2005-14.

54. Rouan, F., et al., *Divergent effects of two sequence variants of GJB3 (G12D and R32W) on the function of connexin 31 in vitro.* Exp Dermatol, 2003. 12(2): p. 191-7.

55. Kelsell, D.P., et al., *Connexin 26 mutations in hereditary non-syndromic sensorineural deafness.* Nature, 1997. 387(6628): p. 80-3.

56. Mese, G., G. Richard, and T.W. White, *Gap junctions: basic structure and function.* J Invest Dermatol, 2007. 127(11): p. 2516-24.

57. Kenneson, A., K. Van Naarden Braun, and C. Boyle, *GJB2 (connexin 26) variants and nonsyndromic sensorineural hearing loss: a HuGE review.* Genet Med, 2002. 4(4): p. 258-74.

58. Davidson, J., M.L. Hyde, and P.W. Alberti, *Epidemiologic patterns in childhood hearing loss: a review.* Int J Pediatr Otorhinolaryngol, 1989. 17(3): p. 239-66.

59. Marazita, M.L., et al., *Genetic epidemiological studies of early-onset deafness in the U.S. school-age population.* Am J Med Genet, 1993. 46(5): p. 486-91.

60. Kikuchi, T., et al., *Gap junction systems in the rat vestibular labyrinth: immunohistochemical and ultrastructural analysis.* Acta Otolaryngol, 1994. 114(5): p. 520-8.

61. del Castillo, I., et al., *A deletion involving the connexin 30 gene in nonsyndromic hearing impairment.* N Engl J Med, 2002. 346(4): p. 243-9.

62. Oguchi, T., et al., *Clinical features of patients with GJB2 (connexin 26) mutations: severity of hearing loss is correlated with genotypes and protein expression patterns.* J Hum Genet, 2005. 50(2): p. 76-83.

63. Alexandrino, F., et al., *G59S mutation in the GJB2 (connexin 26) gene in a patient with Bart-Pumphrey syndrome.* Am J Med Genet A, 2005. 136(3): p. 282-4.

64. Common, J.E., et al., *Specific loss of connexin 26 expression in ductal sweat gland epithelium associated with the deletion mutation del(GJB6-D13S1830).* Clin Exp Dermatol, 2005. 30(6): p. 688-93.

65. Yotsumoto, S., et al., *Novel mutations in GJB2 encoding connexin-26 in Japanese patients with keratitis-ichthyosis-deafness syndrome.* Br J Dermatol, 2003. 148(4): p. 649-53.

66. Lee, J.R. and T.W. White, *Connexin-26 mutations in deafness and skin disease.* Expert Rev Mol Med, 2009. 11: p. e35.

67. Burns, F., *A case of generalized keratoderma with unusual involvement of eyes and nasal and buccal mucous membranes.* J Cutan Dis, 1915. 33: p. 255-260.

68. Skinner, B.A., M.C. Greist, and A.L. Norins, *The keratitis, ichthyosis, and deafness (KID) syndrome.* Arch Dermatol, 1981. 117(5): p. 285-9.

69. Caceres-Rios, H., et al., *Keratitis, ichthyosis, and deafness (KID syndrome): review of the literature and proposal of a new terminology.* Pediatr Dermatol, 1996. 13(2): p. 105-13.

70. Coggshall, K., et al., *Keratitis, ichthyosis, and deafness syndrome: a review of infectious and neoplastic complications.* J Am Acad Dermatol, 2013. 69(1): p. 127-34.

71. Harms, M., et al., *KID syndrome (keratitis, ichthyosis, and deafness) and chronic mucocutaneous candidiasis: case report and review of the literature.* Pediatr Dermatol, 1984. 2(1): p. 1-7.

72. Williams, M.L. and T.H. McCalmont, *KID versus KED: What's in a name.* Pediatr Dermatol, 1996. 13(2): p. 154-7.

73. Maintz, L., et al., *Keratitis-ichthyosis-deafness syndrome in association with follicular occlusion triad.* Eur J Dermatol, 2005. 15(5): p. 347-52.

74. Montgomery, J.R., et al., *A novel connexin 26 gene mutation associated with features of the keratitis-ichthyosis-deafness syndrome and the follicular occlusion triad.* J Am Acad Dermatol, 2004. 51(3): p. 377-82.

75. Todt, I., et al., *Neurotological and neuroanatomical changes in the connexin-26-related HID/KID syndrome.* Audiol Neurootol, 2006. 11(4): p. 242-8.

76. Werchau, S., et al., *Keratitis-ichthyosis-deafness syndrome: response to alitretinoin and review of literature.* Arch Dermatol, 2011. 147(8): p. 993-5.

77. Zhang, X., et al., *Severe ichthyosis-related disorders in children: response to acitretin.* J Dermatolog Treat, 2007. 18(2): p. 118-22.

78. Miteva, L., *Keratitis, ichthyosis, and deafness (KID) syndrome.* Pediatr Dermatol, 2002. 19(6): p. 513-6.

79. Haruna, K., et al., *Severe form of keratitis-ichthyosis-deafness (KID) syndrome associated with septic complications.* J Dermatol, 2010. 37(7): p. 680-2.

80. Hazen, P.G., et al., *Keratitis, ichthyosis, and deafness (KID) syndrome: management with chronic oral ketoconazole therapy.* Int J Dermatol, 1992. 31(1): p. 58-9.

81. Mazereeuw-Hautier, J., et al., *Keratitis-ichthyosis-deafness syndrome: disease expression and spectrum of connexin 26 (GJB2) mutations in 14 patients.* Br J Dermatol, 2007. 156(5): p. 1015-9.

82. Alvarez, A., et al., *De novo mutation in the gene encoding connexin-26 (GJB2) in a sporadic case of keratitis-ichthyosis-deafness (KID) syndrome.* Am J Med Genet A, 2003. 117A(1): p. 89-91.

83. Restano, L., S. Cambiaghi, and G. Tadini, *The pattern of inheritance in KID syndrome.* Pediatr Dermatol, 1999. 16(2): p. 164-5.

84. Richard, G., et al., *Missense Mutations in GJB2 Encoding Connexin-26 Cause the Ectodermal Dysplasia Keratitis-Ichthyosis-Deafness Syndrome.* Am J Hum Genet, 2002. 70(5): p. 1341-8.

85. Gerido, D.A., et al., *Aberrant hemichannel properties of Cx26 mutations causing skin disease and deafness.* Am J Physiol Cell Physiol, 2007. 293(1): p. C337-45.

86. Lee, J.R., A.M. Derosa, and T.W. White, *Connexin mutations causing skin disease and deafness increase hemichannel activity and cell death when expressed in Xenopus oocytes.* J Invest Dermatol, 2009. 129(4): p. 870-8.

87. Aypek, H., V. Bay, and G. Mese, *Altered cellular localization and hemichannel activities of KID syndrome associated connexin26 I30N and D50Y mutations.* BMC Cell Biol, 2016. 17: p. 5.

88. Terrinoni, A., et al., *Connexin 26 (GJB2) mutations, causing KID Syndrome, are associated with cell death due to calcium gating deregulation.* Biochem Biophys Res Commun, 2010. 394(4): p. 909-14.

89. Garcia, I.E., et al., *Keratitis-ichthyosis-deafness syndrome-associated Cx26 mutants produce nonfunctional gap junctions but hyperactive hemichannels when co-expressed with wild type Cx43.* J Invest Dermatol, 2015. 135(5): p. 1338-47.

90. Schutz, M., et al., *The connexin26 S17F mouse mutant represents a model for the human hereditary keratitis-ichthyosis-deafness syndrome.* Hum Mol Genet, 2011. 20(1): p. 28-39.

91. Mese, G., et al., *The Cx26-G45E mutation displays increased hemichannel activity in a mouse model of the lethal form of keratitis-ichthyosis-deafness syndrome.* Mol Biol Cell, 2011. 22(24): p. 4776-86.

92. Fang, H. and F. Beier, *Mouse models of osteoarthritis: modelling risk factors and assessing outcomes.* Nat Rev Rheumatol, 2014. 10(7): p. 413-21.

93. El Ghalbzouri, A., et al., *Leiden reconstructed human epidermal model as a tool for the evaluation of the skin corrosion and irritation potential according to the ECVAM guidelines.* Toxicol In Vitro, 2008. 22(5): p. 1311-20.

94. Brohem, C.A., et al., *Artificial skin in perspective: concepts and applications.* Pigment Cell Melanoma Res, 2011. 24(1): p. 35-50.

95. Wong, T., J.A. McGrath, and H. Navsaria, *The role of fibroblasts in tissue engineering and regeneration.* Br J Dermatol, 2007. 156(6): p. 1149-55.

96. Olah, A., A.G. Szollosi, and T. Biro, *The channel physiology of the skin.* Rev Physiol Biochem Pharmacol, 2012. 163: p. 65-131.

97. Rawlings, A.V., *Recent advances in skin 'barrier' research.* J Pharm Pharmacol, 2010. 62(6): p. 671-7.

98. McLachlin, J.R., et al., *Factors affecting retroviral vector function and structural integrity.* Virology, 1993. 195(1): p. 1-5.

99. Kim, T.K. and J.H. Eberwine, *Mammalian cell transfection: the present and the future.* Anal Bioanal Chem, 2010. 397(8): p. 3173-8.

100. Deyrieux, A.F. and V.G. Wilson, *In vitro culture conditions to study keratinocyte differentiation using the HaCaT cell line.* Cytotechnology, 2007. 54(2): p. 77-83.

101. Jara, O., et al., *Critical role of the first transmembrane domain of Cx26 in regulating oligomerization and function.* Mol Biol Cell, 2012. 23(17): p. 3299-311.

102. Saffitz, J.E., J.G. Laing, and K.A. Yamada, *Connexin expression and turnover : implications for cardiac excitability.* Circ Res, 2000. 86(7): p. 723-8.

103. Celetti, S.J., et al., *Implications of pannexin 1 and pannexin 3 for keratinocyte differentiation.* J Cell Sci, 2010. 123(Pt 8): p. 1363-72.

104. Schoop, V.M., N. Mirancea, and N.E. Fusenig, *Epidermal organization and differentiation of HaCaT keratinocytes in organotypic coculture with human dermal fibroblasts.* J Invest Dermatol, 1999. 112(3): p. 343-53.

105. Ryle, C.M., et al., *Density-dependent modulation of synthesis of keratins 1 and 10 in the human keratinocyte line HACAT and in ras-transfected tumorigenic clones.* Differentiation, 1989. 40(1): p. 42-54.

106. Deyrieux, A.F. and V.G. Wilson, *In vitro culture conditions to study keratinocyte differentiation using the HaCaT cell line.* Cytotechnology, 2007. 54(2): p. 77-83.

107. Wilson, V.G., *Growth and differentiation of HaCaT keratinocytes.* Methods Mol Biol, 2014. 1195: p. 33-41.

108. Matos, T.D., et al., *A novel M163L mutation in connexin 26 causing cell death and associated with autosomal dominant hearing loss.* Hear Res, 2008. 240(1-2): p. 87-92.

109. Ravi, M., et al., *3D cell culture systems: advantages and applications.* J Cell Physiol, 2015. 230(1): p. 16-26.

110. Pereira, R.F., et al., *Advanced biofabrication strategies for skin regeneration and repair.* Nanomedicine (Lond), 2013. 8(4): p. 603-21.

111. Chau, D.Y., et al., *The development of a 3D immunocompetent model of human skin.* Biofabrication, 2013. 5(3): p. 035011.

112. Ng, K., et al., *Paper-based cell culture platform and its emerging biomedical applications.* Materials Today, 2017. 20(1): p. 32-44.